Praseodymium-Doped $Sr_2TiFeO_{6-\delta}$ Double Perovskite as a Bi-Functional Electrocatalyst for Hydrogen Production Through Water Splitting

By

Qassam Sarmad

Reg. No 00000274120

Session 2018-20

Supervised by

Dr. Mustafa Anwar

US-Pakistan Center for Advanced Studies in Energy (USPCAS-E)

National University of Sciences and Technology (NUST)

H-12, Islamabad 44000, Pakistan

March 2022

Praseodymium-Doped $Sr_2TiFeO_{6-\delta}$ Double Perovskite as a Bi-Functional Electrocatalyst for Hydrogen Production Through Water Splitting

By

Qassam Sarmad

Reg. No 00000274120

Session 2018-20

Supervised by

Dr. Mustafa Anwar

A Thesis Submitted to the US-Pakistan Center for Advanced Studies in Energy in partial fulfillment of the requirements for the degree of MASTERS of SCIENCE in ENERGY SYSTEMS ENGINEERING

US-Pakistan Center for Advanced Studies in Energy (USPCAS-E)

National University of Sciences and Technology (NUST)

H-12, Islamabad 44000, Pakistan

March 2022

THESIS ACCEPTANCE CERTIFICATE

Certified that final copy of MS/MPhil thesis written by Mr. Qassam Sarmad (Registration No. 00000274120), of USPCAS-E has been vetted by undersigned, found complete in all respects as per NUST Statues/Regulations, is within the similarity indices limit and is accepted as partial fulfillment for the award of MS/MPhil degree. It is further certified that necessary amendments as pointed out by GEC members of the scholar have also been incorporated in the said thesis.

Signature: _____

Name of Supervisor: Dr. Mustafa Anwar ……

Date: _____

Signature (HoD): _____

Date: _____

Signature (Dean/Principal): _____

Date: _____

Certificate

This is to certify that work in this thesis has been carried out by **Mr. Qassam Sarmad** and completed under my supervision in AEMS laboratory, US-Pakistan Center for Advanced Studies in Energy (USPCAS-E), National University of Sciences and Technology, H-12, Islamabad, Pakistan.

Supervisor: _____

Dr. Mustafa Anwar
USPCAS-E
NUST, Islamabad

Co-supervisor: zskhan
_____

Prof. Dr. Zuhair S. Khan
USPCAS-E
NUST, Islamabad

GEC member 2: _____

Prof. Dr. Naseem Iqbal
USPCAS-E
NUST, Islamabad

GEC member 3: _____

Dr. Asif Hussain Khoja
USPCAS-E
NUST, Islamabad

HOD-ESE: _____

Dr. Rabia Liaquat
USPCAS-E
NUST, Islamabad

Dean/Principal: _____

Prof. Dr. Adeel Waqas
USPCAS-E
NUST, Islamabad

Dedication

I would like to wholeheartedly dedicate my thesis to my beloved parents, who have been a constant source of inspiration and strength and continuously provided their moral, spiritual, and emotional support.

Abstract

Water Splitting by electrocatalysis is one method of attaining sustainable production of hydrogen as a clean and promising energy source. Previous studies have shown that perovskite can be effective electrocatalyst for overall water splitting. Herein, double perovskites being highly stable structures have been reported to perform exceptionally in harsh electrochemical environments. The Praseodymium (Pr) doped Strontium Titanium Ferrite (STF) electrocatalyst was tested as an electrocatalyst for water splitting with conductive nickel foam. Pr was doped both on A and B sites of the STF's double perovskite structure, and the $SrTiFe_{0.9}Pr_{0.1}O_{6-\delta}$ (STFP01) showed the best results with an oxygen evolution reaction (OER) overpotential of 277.6 mV@ 5 mV/s and a hydrogen evolution reaction (HER) overpotential of 182.4 mV@ 5 mV/s with low Tafel slopes of 73 mV/dec and 77 mV/dec, respectively. The sponge-like structure of Pr-doped STF exhibits excellent potential to be a viable electrocatalyst while providing a stable structure.

Keywords: *Water splitting; Double Perovskite; Hydrogen Evolution Reaction (HER); Oxygen Evolution Reaction (OER); Hydrogen Production*

Table of Contents

List of Figures

List of Tables

List of Publications

1. **Qassam Sarmad**, Uneeb Masood Khan, Mutawara Mahmood Baig, Muhammad Hassan, Faaz Ahmed Butt, Asif Hussain Khoja, Rabia Liaquat, Zuhair S. Khan, Mustafa Anwar*, Muhammad Ali S.A. “Praseodymium-doped $Sr_2TiFeO_{6-\delta}$ double perovskite as a bi-functional electrocatalyst for hydrogen production through water splitting.” *Journal of Environmental Chemical Engineering*
2. Uneeb Masood Khan, **Qassam Sarmad**, Mustafa Anwar*, Asif Hussain Khoja, Muhammad Ali S.A., Zuhair S. Khan, Muhammad Hassan, Sehar Shakir. “Synthesis of cobalt loaded double perovskite $Sr_2TiFeO_{6-\delta}$ (STF) as a stable catalyst for enhanced hydrogen production via methane decomposition.” *International Journal of Energy Research*, vol. 45, no. 14, 2021, pp. 20073-20088, https://doi.org/10.1002/er.7084
3. **Qassam Sarmad**, Uneeb Masood Khan, Mustafa Anwar, A. H. Khoja, M. Ali, Z. S. Khan, Andanastuti Muchtar*, and M. R. Somalu. "Catalytic Performance of Calcium-Lanthanum co-doped Ceria ($Ce_{0.85-x}La_{0.15}Ca_xO_{2-\delta}$) in Partial Oxidation of Methane." *Bulletin of Chemical Reaction Engineering & Catalysis*, vol. 16, no. 3, 2021, pp. 548-554, https://doi.org/10.9767/bcrec.16.3.10528.548-554
4. Amer Zaffar, Bilal Alam Khan, Asif Hussain Khoja*, Uneeb Masood Khan, **Qassam Sarmad**, Muhammad Taqi Mehran, Salman Raza Naqvi, and Majid Ali. "Synthesis of Ash Derived Co/Zeolite Catalyst for Hydrogen Rich Syngas Production via Partial Oxidation of Methane." *Bulletin of Chemical Reaction Engineering & Catalysis*, vol. 16, no. 3, 2021, pp. 507-516, https://doi.org/10.9767/bcrec.16.3.10614.507-516

List of Abbreviations

BET	Brunauer – Emmett – Teller surface area analysis
BJH	Barrett, Joyner, and Halenda method
CV	Cyclic voltammetery
EDS	Energy-dispersive X-ray spectroscopy
EIS	Impedance electroscopy
GHGs	Greenhouse gases
HER	Hydrogen evolution reaction
LSV	Linear sweep voltammetery
OER	Oxygen evolution reaction
RHE	Reversible hydrogen electrode
SEM	Scanning electron microscopy
STF	$Sr_2TiFeO_{6-\delta}$
TGA	Thermogravimetric analysis
XRD	X-ray diffraction

Chapter 1: Introduction

1.1 Overview of Research

Energy is a necessary commodity in today's world, which has only been increasing in demand every year. As the technology progresses, the demand for energy increases with it. For over the past 150 years or so, fossil fuels have provided a very large and significant energy storage. Coal, Oil and Natural gas are very dense fuels in terms of energy which can be stored easily in solid, liquid or gaseous states. This means that as per requirement of the demand side of the energy system, the energy stored in fossil fuels can be called upon. For example, when the demand of electricity increases, more fuel can be put into the power plant for increased generation of electricity. This is significant because the access to on-demand energy provided by the fossil fuels has made the current energy system very inflexible as the consumers on the demand side of the system expect the energy to be available as and when they need it.

However, there are a certain number of factors today that make fossil fuels less than ideal today. Fossil fuels may have been once present in abundance, but they are depleting fast [1]. This automatically becomes a problem because most of the technology today relies heavily on fossil fuels for energy generation. Most of the engines and turbines in the world depend upon the combustion of one fossil fuel or the other.

Secondly, for quite some time, a part of the scientific community has been warning the world about the dangers of the excessive use fossil fuels due to the harmful pollutants they release. And undoubtedly, this has become a major issue in the world today, with Global Warming and Climate Change on the rise.

The main human CO_2 addition to the atmosphere is from the burning of fossil fuels. The ocean is estimated to be absorbing 2.0 ± 0.8 Gt/year of CO_2, which is the cause of acidification that in turn harms the coral reefs and other systems. This combined with the CO_2 generation due to cement manufacturing, forest clearance and soil disturbance has led to an imbalance in the current CO_2 concentration in the atmosphere that has not existed for over a million years. This increased energy

retention in the Earth's system has resulted in a global 0.8 °C rise in the global average temperature. This seemingly small change in average conditions has already increased the occurrence and the intensity of extreme weather events such as severe storms, floods, droughts and heat waves. The probability of initiating catastrophic climate change will be at least one in five if 565 more gigatons of CO_2 are added to the atmosphere. Fossil fuel combustion must be reduced by 90% by 2050 in order to have a chance of avoiding a run-away climate change. Recent estimates for the known economically recoverable reserves of fossil fuels would produce around 2795 Gt of CO_2. This means a certain climate catastrophe if the world continues on its current path [2].

Issues like these have sent the researchers and the innovators of the world on a quest for alternative fuel to replace the traditional fossil fuels that we have been using for decades now. The push for Electric Vehicles, Solar Power Plants, Wind Turbine farms and other such initiatives is a testament to the commitment of the community vying for a change.

The concept of hydrogen economy was first proposed by the revolutionary author Jules Verne in 1870s as a speculation in his novel, The Mysterious Island [3]. The term "hydrogen economy", a common term today was first used by Mr. John Bockris in 1970 at a presentation in General Motors. The concept of hydrogen economy is that hydrogen will be produced using the already available energy sources. The hydrogen will then replace the fossil fuels being currently used commercially in industries, residences and transportation. The proposed idea of the hydrogen economy is to be an effective answer to some of the world's most pressing interconnected problems today: (i) global environmental issues, (ii) exhaustion of natural resources, (iii) food scarcity in developing countries, and (iv) ever increasing global population. [4].

Experts from the Institute of Nuclear Energy in Vienna and the Electric Power Research Institute conducted extensive research on hydrogen production in the 1970s [5]. The core idea was to produce hydrogen gas using nuclear reactions and in turn that hydrogen gas will be used to produce electricity. This will ultimately replace fossil fuels. However, the study's findings revealed that producing hydrogen using high temperature thermonuclear methods was more efficient and cost effective

than producing hydrogen via electrolysis [6]. However, the study found that generating electricity directly from nuclear plants was less expensive and more efficient than using hydrogen to produce electricity using a fuel cell.

Although hydrogen is plentiful on Earth, it is mostly chemically bound. For it to be used as a fuel, it must be available in its molecular state or in an unbound form. This is where the major problem lies because a substantial amount of energy is required to obtain hydrogen in its unbound form. The energy required to obtain hydrogen gas is far greater than the energy produced when the same gas is used as fuel, rendering it unfeasible. According to the equation below, 120 MJ/kg-hydrogen is required to break down a water molecule into hydrogen and oxygen. Whereas the reverse reaction ideally yields 120 MJ/kg-hydrogen. Because ideal reactions do not occur in the real world, greater than 120 MJ/kg of useful energy must be put into the first reaction, whereas less than 120 MJ/kg of useful energy is recovered from the recombination.

$$2H_2O \rightarrow 2H_2 + O_2$$

Hydrogen gas can be obtained from fossil fuels, nuclear materials or even renewable sources. There are several processes that can utilized for Hydrogen production such as Fischer-Trope, water-splitting, methane cracking, etc. Depending on the method, the hydrogen produced can either be “Green Hydrogen” or “Non-Green Hydrogen”. Hydrogen can be stored in multiple forms. It can be either stored as gas in cylinders, as liquid or even in metal hydrides. Recent progress in the field has made storage in metal hydrides as feasible and safe [7].

1.2 Problem Statement

Electrochemical water splitting is the cleanest technique to produce H_2 as it leaves zero carbon footprint [8]. The reaction can be broken into 2 half reactions, oxygen evolution reaction (OER) at the anode and hydrogen evolution reaction (HER) at cathode. The reactions are presented in the equation below[9]–[11]:

$$4H^+ + 4e^- \rightarrow 2H_2 \text{ (HER at cathode)} \quad (1.1)$$

$$2H_2O \rightarrow O_2 + 4H^+ + 4e^- \text{ (OER at anode)} \quad (1.2)$$

$$2H_2O \rightarrow O_2 + 2H_2 \quad (1.3)$$

The requirement of large overpotential can said to be the main obstacle for large-scale hydrogen generation through water splitting [12], [13]. A standard potential (ΔE) of 1.23 V against a reversible hydrogen electrode (RHE) is required for the electrolyzer to split water into H_2 and O_2 [14]. Furthermore, the stability of electrocatalysts is another huge hurdle in the commercialization of hydrogen production through water splitting. Since the reaction is carried out in usually either acidic or alkaline electrolytes, the material being used as the catalyst must demonstrate resistance towards degradation over time.

Traditionally, the catalysts being used for HER were expensive metals such as platinum, iridium, palladium, and rhodium which would be extremely difficult to commercialize [15]–[18]. Later research proved transition metals such as iron, nickel, and cobalt to be extremely effective, and being cheaper they can be easily replaced if they degrade under stronger acidic or alkaline conditions [19]–[21]. In recent years, numerous studies have been published using different types of compounds consisting of multiple elements to find effective electrodes for electrochemical water splitting.

1.3 Hypothesis

Double perovskites have been shown to be stable under acidic and alkaline catalytic conditions. Pr^{3+} ions have been reported to play a significant role in increasing the oxygen vacancy of the lattice and have yielded favorable results in recent studies [22]. Praseodymium was doped in the double perovskite structure of STF on both the A-site and the B-site to see if it affected the performance of the synthesized electrocatalysts. Hence, in this study Pr-doped STF will be synthesized through Pechini method, as it has been proven to yield porous structures and high surface areas. The double perovskite structure of Pr-doped STF should also be stable under the alkaline conditions of electrocatalysis. Pr-STF should perform excellently as a water splitting catalyst and should be stable as well.

1.4 Objectives

The objectives of this study are:

1. To synthesize and characterize Praseodymium doped $Sr_2TiFeO_{6-\delta}$, a double perovskite catalyst
2. To analyze the effect of Pr-doping on structural and morphological properties of STF double perovskite
3. To study the performance of Pr-doped STF as an electrocatalyst in water splitting reactions

1.5 Scope of Work

Pr-doped STF was synthesized using the Pechini method, and the as synthesized samples were characterized using thermogravimetric analysis (TGA), X-ray diffraction (XRD), field emission scanning electron microscopy (FESEM), energy-dispersive X-ray spectroscopy (EDS) and N_2 physisorption. Electrochemical measurements were carried out to determine the water splitting potential on an electrochemical workstation. Two and three-electrode assemblies were tested for the materials on the workstation to find out the overall water splitting potential. The working electrodes were made from drop casting the catalyst inks onto nickel foam, Ag/AgCl was used as the reference electrode and Platinum wire was used as the counter electrode. All electrocatalysts with varying Pr doping were electrochemically measured in 2 M KOH solution at varying scan rates. The best performing sample was also tested for stability for 12 hours and 1000 cycles.

1.6 Outline

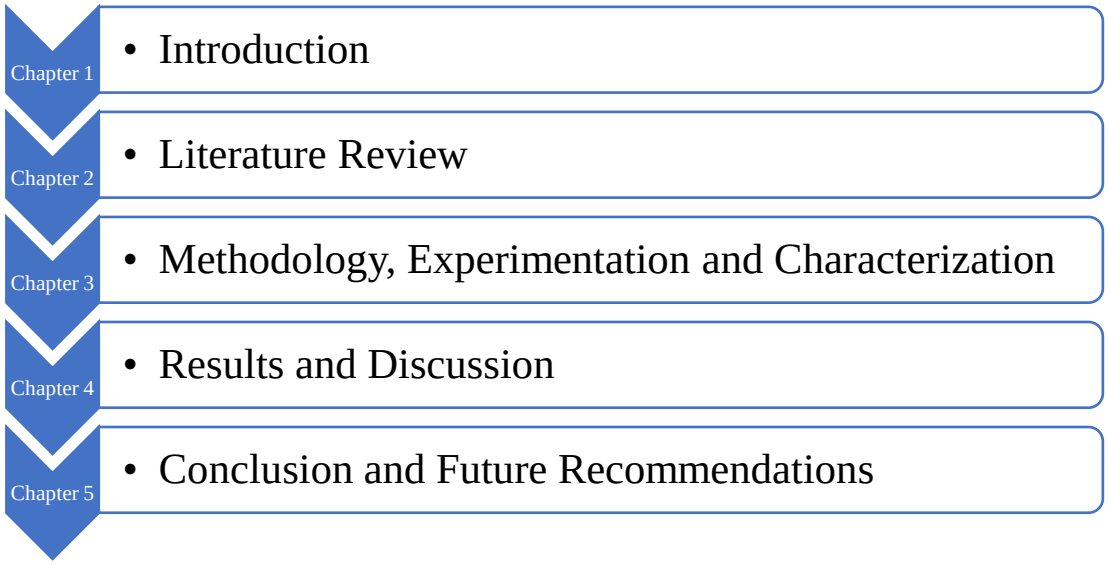

Summary

Energy shortages and climate change are two of the key problems the world is facing currently. Both of these can be effectively addressed if green hydrogen can be made commercially viable. Hydrogen gas can be obtained from a number of sources, but in order to make it environmentally friendly or green, water splitting is the go-to technique. Researchers have been working on materials that can effectively produce H_2 from water at lower costs. In this regard, perovskites and double perovskites have been gaining some popularity recently, as they are highly tunable and very stable under harsh conditions.

The focus of this study is to synthesize Pr-doped STF double perovskite and to study its performance as an electrocatalyst for water splitting reactions, namely, HER and OER. The doping of Pr was varied to determine its effect on the material's electrochemical performance. The as-synthesized samples were characterized using TGA, XRD, FESEM, EDS and BET.

References

[1] M. Höök *et al.*, "Depletion of fossil fuels and anthropogenic climate change—A review," *Energy Policy*, vol. 52, pp. 797–809, Jan. 2013, doi: 10.1016/J.ENPOL.2012.10.046.

[2] F. Kreith *et al.*, "Principles of Sustainable Energy Systems," *Sustain. Energy*, 2010, doi: 10.4324/9780203841563.

[3] J. Verne, *The Mysterious Island*. New York, 1888.

[4] J. O. Abe *et al.*, "Hydrogen energy, economy and storage: Review and recommendation," *Int. J. Hydrogen Energy*, vol. 44, no. 29, pp. 15072–15086, Jun. 2019, doi: 10.1016/J.IJHYDENE.2019.04.068.

[5] R. Shinnar, "The hydrogen economy, fuel cells, and electric cars," *Technology in Society*. 2003, doi: 10.1016/j.techsoc.2003.09.024.

[6] F. Kreith *et al.*, "Fallacies of a hydrogen economy: A critical analysis of hydrogen production and utilization," 2004.

[7] I. Dincer *et al.*, *Sustainable Hydrogen Production*. 2016.

[8] J. Yin *et al.*, "Optimized metal chalcogenides for boosting water splitting," *Adv. Sci.*, vol. 7, no. 10, p. 1903070, 2020.

[9] C. G. Morales-Guio *et al.*, "Nanostructured hydrotreating catalysts for electrochemical hydrogen evolution," *Chemical Society Reviews*. 2014, doi: 10.1039/c3cs60468c.

[10] Y. Li, H. Wang *et al.*, "MoS_2 nanoparticles grown on graphene: An advanced catalyst for the hydrogen evolution reaction," *J. Am. Chem. Soc.*, 2011, doi: 10.1021/ja201269b.

[11] B. You *et al.*, "Enhancing electrocatalytic water splitting by strain engineering," *Adv. Mater.*, vol. 31, no. 17, p. 1807001, 2019.

[12] H. Sun *et al.*, "Designing High-Valence Metal Sites for Electrochemical Water Splitting," *Adv. Funct. Mater.*, vol. 31, no. 16, pp. 1–44, 2021, doi: 10.1002/adfm.202009779.

[13] J. Yu *et al.*, "Recent advances and prospective in ruthenium-based materials for electrochemical water splitting," *Acs Catal.*, vol. 9, no. 11, pp. 9973–10011, 2019.

[14] J. Zhang *et al.*, "Support and interface effects in water-splitting electrocatalysts," *Adv. Mater.*, vol. 31, no. 31, p. 1808167, 2019.

[15] D. W. Lima *et al.*, “PtNi and PtMo nanoparticles as efficient catalysts using TEA-PS.BF_4 ionic liquid as electrolyte towards HER,” *Int. J. Hydrogen Energy*, 2017, doi: 10.1016/j.ijhydene.2016.11.166.

[16] X. Cheng *et al.*, “Highly active, stable oxidized platinum clusters as electrocatalysts for the hydrogen evolution reaction,” *Energy Environ. Sci.*, 2017, doi: 10.1039/c7ee02537h.

[17] J.-W. Tian *et al.*, “A new 2D Co_5-cluster based MOF: Crystal structure, magnetic properties and electrocatalytic hydrogen evolution reaction,” *Inorg. Chem. Commun.*, vol. 95, pp. 73–77, 2018.

[18] Y. Li *et al.*, “Recent advances on water-splitting electrocatalysis mediated by noble-metal-based nanostructured materials,” *Adv. Energy Mater.*, vol. 10, no. 11, p. 1903120, 2020.

[19] M. H. Miles *et al.*, “Periodic Variations of Overvoltages for Water Electrolysis in Acid Solutions from Cyclic Voltammetric Studies,” *J. Electrochem. Soc.*, 1976, doi: 10.1149/1.2132619.

[20] S. Hu *et al.*, “Ni_3N/NF as Bifunctional Catalysts for Both Hydrogen Generation and Urea Decomposition,” *ACS Appl. Mater. Interfaces*, 2019, doi: 10.1021/acsami.8b19052.

[21] W. Zhao *et al.*, “Novel Cobalt-Doped $Ni_{0.85}Se$ Chalcogenides ($Co_xNi_{0.85-x}Se$) as High Active and Stable Electrocatalysts for Hydrogen Evolution Reaction in Electrolysis Water Splitting,” *ACS Appl. Mater. Interfaces*, 2018, doi: 10.1021/acsami.8b12797.

[22] S. Ward *et al.*, “Boosting the oxygen evolution activity in non-stoichiometric praseodymium ferrite-based perovskites by A site substitution for alkaline electrolyser anodes,” *Sustain. Energy Fuels*, 2021, doi: 10.1039/d0se01278e.

Chapter 2: Literature Review

2.1 Overview

Fossil fuels are depleting and would not last even for the foreseeable future as the main source of energy globally. Researchers have long been trying to find alternative fuels, that are sustainable and eco-friendly. Hydrogen leads this race as a potential source of energy that can sustainably cater to the needs of the world. H_2 gas has an exceedingly superior energy density of nearly 142 MJ/kg, and upon combustion, it only produces water as the by-product making it highly clean[1], [2]. Hydrogen is the amplest element in the entire of the known universe, but it is not often observed on its own as H_2 gas. As a result, it must be produced in another way and stored so that it can be used effectively as and when required.

Furthermore, Hydrogen gas as a fuel is far more efficient as compared to the conventional fuels that are common in the world today as summarized in Table 2-1 [3]. Hydrogen gas is widely recognized as an environmentally friendly secondary form of renewable energy and an alternative to fossil fuels because it is not only carbon-free but also has the highest energy content [4]–[6]. Another advantage is that, with appropriate storage systems, hydrogen is suitable for domestic use because it can be transported consistently via standard means [7]–[10]. It can also be stored as compressed gas, cryogenic liquid, or solid hydride for use in fuel cells [11]–[13].

Table 2-1 - Comparison of HHV and LHV of common fuels [3]

Fuel	State at ambient conditions	HHV (MJ/kg)	LHV (MJ/kg)
Hydrogen	Gas	141.9	119.9
Methane	Gas	55.5	50
Ethane	Gas	51.9	47.8
Gasoline	Liquid	47.5	44.5
Diesel	Liquid	44.8	42.5
Methanol	Liquid	20	18.1

2.2 Hydrogen Production

Based on the type of raw materials being used, hydrogen production can be separated into two general classifications: conventional and renewable technologies. Traditional methods rely on fossil fuels and include techniques like hydrocarbon reforming and pyrolysis. Chemical techniques such as steam reforming, partial

oxidation, and autothermal steam reforming can be used to further refine hydrocarbon reforming.

The second major category, as the name implies, includes techniques for producing hydrogen from renewable resources, such as biomass or water. Techniques that use biomass as a feedstock for hydrogen production are further classified into two types: thermochemical processes and biological processes. Pyrolysis, gasification, combustion, and liquefaction are examples of thermochemical processes. Direct and indirect bio-photolysis, dark fermentation, photo-fermentation, and sequential dark & photo-fermentation are among the biological processes. Hydrogen production via water splitting involves processes such as electrolysis, thermolysis, and photo-electrolysis. Water is the only raw material used in these techniques. These various hydrogen production techniques are depicted in Fig. 2-1 [14].

Hydrogen or H_2 as fuel can also be categorized according to how environmentally clean the production methods are. In other words, methods producing the most Carbon can be classified as “grey”, methods involving Carbon Capture and Storage (CCS) can be classified as “blue”, and methods that emit zero carbon are “green”[15]. This classification helps in identifying the impact H_2 production has on the environment. Traditionally, “grey hydrogen” is produced from techniques such as coal gasification, steam reforming of methane, partial oxidation of methane, and methane decomposition. These techniques are cheaper at this point in time, but they leave a considerable amount of carbon footprint on the environment which defeats the purpose of hydrogen as a clean fuel for the future. “Blue hydrogen”, uses the same techniques as “grey hydrogen” but at the same time, it employs carbon capture and storage techniques (CCS). Lastly, “green hydrogen” is the cleanest of the three as it uses techniques that produce H_2 gas purely from water through electrocatalysis, photocatalysis, photoelectrocatalysis, or similar methods that use electricity to split water in H_2 and O_2 gases [16], [17]. “Grey hydrogen” is the most economical right now, however, “blue hydrogen” can pave the way for the future until “green hydrogen” becomes viable commercially. The hydrogen production techniques categorized according to their environmental impacts are shown in Fig. 2-2 [18].

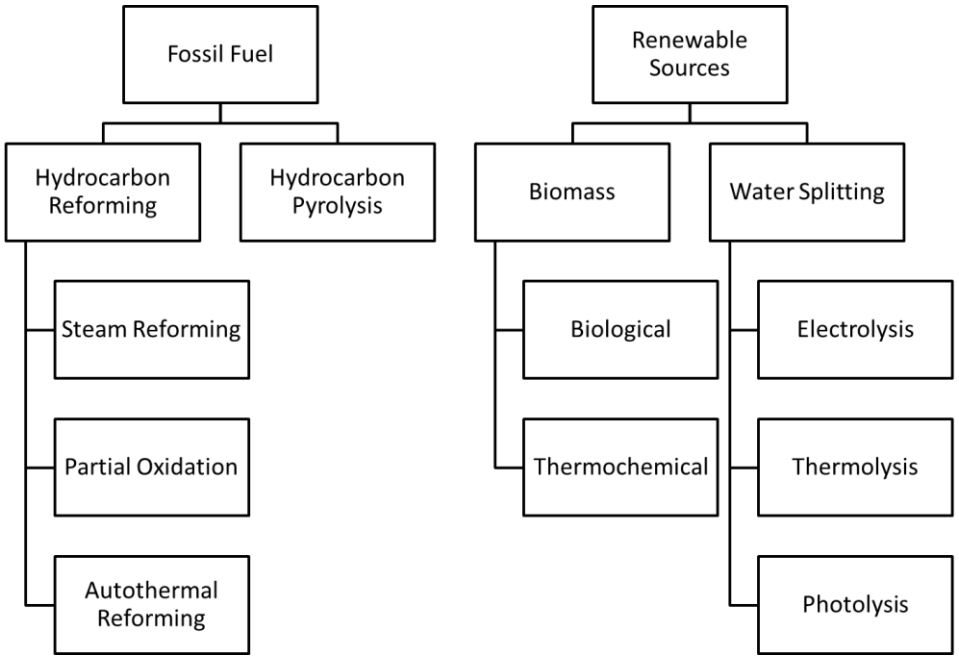

Figure 2-1 - Hydrogen gas production techniques [14]

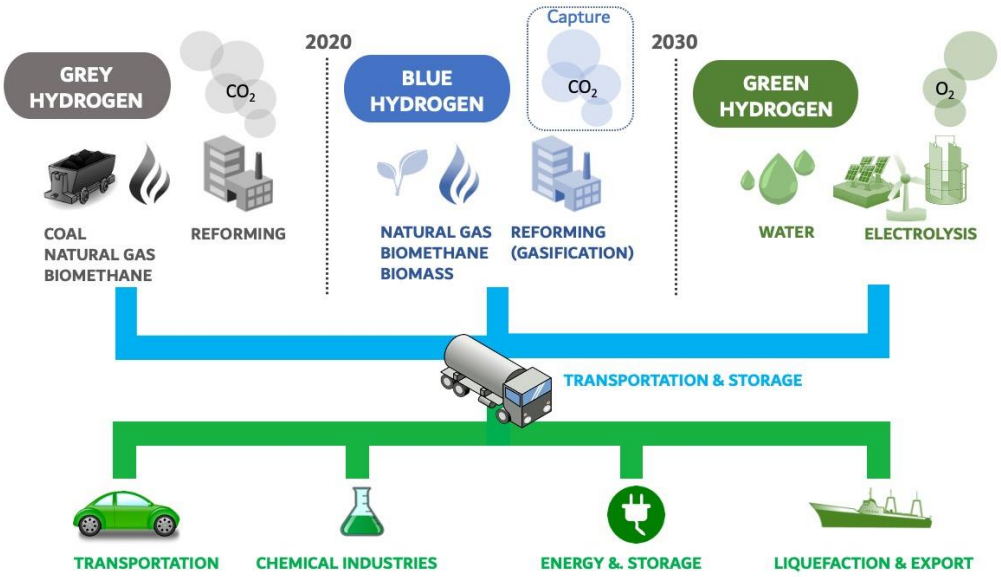

Figure 2-2 - Hydrogen production techniques according to their environmental friendliness [18]

"Green hydrogen", in simple words is produced purely from the electrolysis of water using electricity from renewable sources such as solar, wind, hydro, etc. Currently, the cost is the biggest factor preventing the widespread production of "green hydrogen". According to the International Energy Agency, "green hydrogen" costs around $3 to $7.5 per kg as opposed to the hydrogen produced from a technique such as steam reforming of methane which only costs $0.9 to $3.2 per kg

[19]. Alkaline water electrolysis, proton exchange membrane (PEM) electrolyzers, anion exchange membrane (AEM) electrolyzers, and solid oxide electrolysis (SOEC) are the most common techniques being studied today to produce “green hydrogen”.

2.2.1 Electrochemical Water-Splitting

Electrochemical water splitting is the cleanest technique to produce H_2 as it leaves zero carbon footprint [20]. The reaction can be broken into 2 half reactions, oxygen evolution reaction (OER) at the anode and hydrogen evolution reaction (HER) at cathode. The reactions are presented in the equation below [21]–[23]:

$4H^+ + 4e^- \rightarrow 2H_2$ (HER at cathode)

$2H_2O \rightarrow O_2 + 4H^+ + 4e^-$ (OER at anode)

$2H_2O \rightarrow O_2 + 2H_2$

Theoretically, for water splitting to be done successfully in the electrolyzer, a Gibbs free energy (ΔG) of around 237.2 kJ/mol and a standard potential (E) of 1.23 V is required [24]. However, unfavorable thermodynamics and the requirement of large overpotential are the main obstacle for large-scale hydrogen generation through water splitting [25], [26].

Traditionally, the catalysts being used for HER were expensive metals such as platinum, iridium, palladium, and rhodium which would be extremely difficult to commercialize [27]–[30]. Later research proved transition metals such as iron, nickel, and cobalt to be extremely effective, and being cheaper they can be easily replaced if they corrode under stronger acidic or alkaline conditions [31]–[33]. In recent years, numerous studies have been published using different types of compounds consisting of multiple elements to find effective electrodes for electrochemical water splitting.

2.2.1.1 Mechanisms for Water-Splitting

The fundamental steps in the Hydrogen Evolution Reaction (HER) based on experimental and research data includes these steps [26]:

In acidic media:

$e^- + H^+ + * \rightarrow H^*$

(the Volmer reaction, electrochemical adsorption, ≈ 120 mV dec^{-1})

$H^+ + H^* + e^- \rightarrow H_2$

(the Heyrovsky reaction, electrochemical desorption, ≈ 40 mV dec^{-1})

$H^* + H^* \rightarrow H_2 + 2^*$

(the Tafel reaction, chemical desorption, ≈ 30 mV dec^{-1})

In alkaline or neutral media:

$H_2O + e^- + * \rightarrow OH^- + H^*$

(the Volmer reaction, electrochemical adsorption, ≈ 120 mV dec^{-1})

$H_2O + H^* + e^- \rightarrow H_2 + OH^-$

(the Heyrovsky reaction, electrochemical desorption, ≈ 40 mV dec^{-1})

$H^* + H^* \rightarrow H_2 + 2^*$

(the Tafel reaction, chemical desorption, ≈ 30 mV dec^{-1})

The * depicts the active site on the surface of the electrocatalyst. During the Volmer step, the surface of the electrocatalysts provides the conditions for the hydrogen atom to be adsorbed onto it. It can combine with another H* during the Tafel reaction and release a H_2 molecule and 2 active sites. Or it can react with H^+ or H_2O in acidic or alkaline media during the Heyrovsky reaction [34]. The mechanism has been pictorially represented in Fig. 2-3.

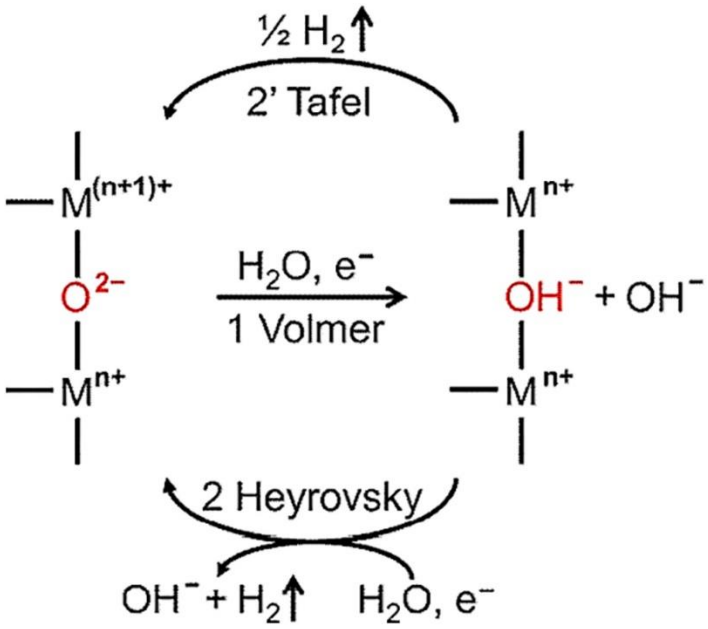

Figure 2-3 - Mechanism proposed for HER on the surface of perovskite oxide [35]

The fundamental steps in the Oxygen Evolution Reaction (OER) based on experimental and research data includes these steps:

In acidic media:

$H_2O + * \rightarrow *OH + e^- + H^+$

$*OH \rightarrow *O + e^- + H^+$

$*O + H_2O \rightarrow *OOH + e^- + H^+$

$*OOH \rightarrow O_2 + e^- + H^+ + *$

In alkaline or neutral media:

$* + OH^- \rightarrow *OH + e^-$

$*OH + OH^- \rightarrow *O + H_2O + e^-$

$*O + OH^- \rightarrow *OOH + e^-$

$*OOH + OH^- \rightarrow O_2 + H_2O + e^- + *$

The * represents the active sites on the surface of the electrocatalysts. In alkaline media, the hydroxyl radical binds to the electrocatalyst's active site to give

*OH. Then, the electron removal from *OH and a coupled proton produces *O. OOH* intermediate is form after that, due to the nucleophilic attack of an OH^- ion onto O*. Lastly, one oxygen molecule is produced along with a free active site after a proton-coupled electron transfer occurs [36].

2.2.1.2 Criteria for an Electrocatalyst

High thermodynamic and kinetic stability, high selectivity, and good stability are the most desired properties for any electrocatalyst [37], [38]. Several methods are used to determine the activity of an electrocatalyst. The most common ones include overpotential at a defined current density, overpotential at a defined mass normalized current density, overpotential at a defined electrochemical surface area (ECSA), normalized current density, Tafel slope, exchange current density and turnover frequency (TOF) [39].

The last three of the parameters listed above are used to determine the reaction kinetics, which tells us about the speed at which the reaction is occurring.

2.3 Common Materials in Electrochemical Water-Splitting

2.3.1 Transition Metal Carbides/Nitrides

This class of electrocatalysts have demonstrated superior conductivity, resistance to corrosion, stability and unique electronic structures that exhibit high efficiency in water electrolysis. Despite of the number of studies done on these materials, when compared to yardstick catalysts such as Pt, Ru, and Ir-based materials, they still have a significant performance gap. Mo and W carbides/nitrides, as well as NiMo and NiFe-based nitrides, have demonstrated great catalytic performance in water splitting. Nevertheless, the stability of these materials is still unsatisfactory [40].

2.3.2 Transition Metal Selenides

In this class of materials, multi-metal selenides and their composites outperform single metal selenides in terms of electrocatalytic performance. Despite their excellent electrochemical performance, stability appears to be an issue with these as well. The selenide-based materials do not appear to last long during HER and OER, which are conducted in highly acidic or basic environments, respectively [41].

2.3.3 Fe-based Metal Organic Framework (MOF)

Fe-MOFs based materials have attracted a lot of attention in the past few years. Aprt from electrochemical applications, these materials have demonstrated good performance in applications such as batteries, super capacitors and CO_2 reduction techniques. Fe-MOFs have exhibited excellent performance in HER and OER and have proven to be versatile in terms of tunability. However, they still have to go a long way before they can be commercialized. Synthesis of Fe-MOFs is highly sensitive, as it is usually done through high-temperature pyrolysis, there is a greater chance of the MOFs precursor being damaged. Also it is important for the Fe-MOF structure to remain intact throughout the HER and OER, as there are no real electrochemically active sites on the structure, and the material depends on the metal nodes to carry out the reaction [42].

2.3.4 Perovskite-Structured Electrocatalysts

Because of their low cost, abundance on Earth, and promising activities, perovskite-type oxides have received a lot of attention [43]–[45]. The general formula for primitive perovskite oxides is ABO_3, in which rare-earth or alkaline metals occupy the A-site and transition metals inhabit the B-site. For water electrolysis, including the basic perovskite oxides (ABO_3), double-(A-site ordered ($A_2BB'O_6$) and B-site ordered ($A_2BB'O_6$)), Ruddlesden–Popper ($A_{n+1}B_nO_{3n+1}$), and quadruple ($AA'_3B_4O_{12}$) types have been investigated [46]–[48], depicted in Fig. 2-4. Perovskite oxides have a flexible structure that can cater to varying amounts of oxygen vacancies and dopants, thus enabling easy modification of their composition. Due to these qualities in perovskite structures, their catalytic performance in water electrolysis is effortlessly tweaked and augmented.

To a considerable degree, the adsorption energies of the intermediate species govern the catalytic action of perovskite oxides, which is usually regulated by the electronic arrangement on surface of the material [50]. First, d-block metal-based perovskite oxides benefit from the peculiar features of 3d valence electrons and in recent times they have gained significant interest for water electrolysis [51]. Furthermore, the metals in the first d-block are reasonably plentiful and inexpensive. As a result, first d-block metal-based perovskite oxides have been widely explored for their potential in water oxidation. [52]. Increasing the use of perovskite oxides in

the hydrogen evolution reaction [35], [53]and overall water splitting reaction [44], [54] has recently gained popularity.

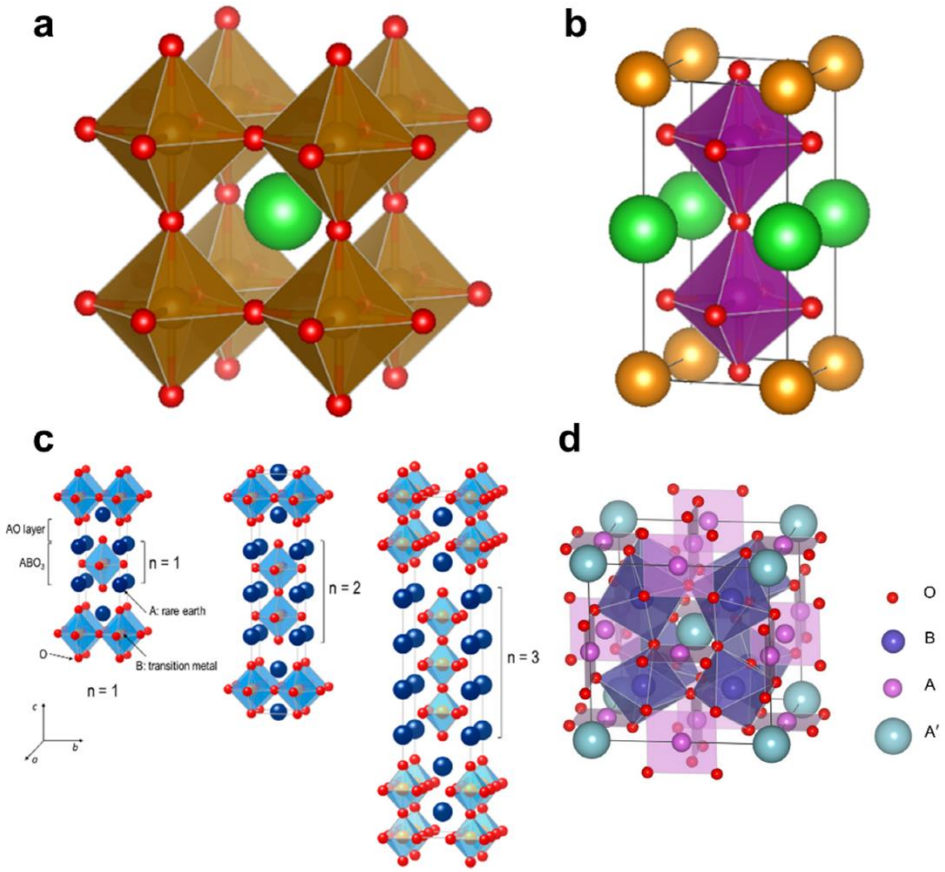

Figure 2-4 Different structures of perovskites (a) Ideal cubic structured perovskite; (b) Tetragonal structured A-site ordered double perovskite; (c) Ruddlesden–Popper structured layered perovskite ($A_{n+1}B_nO_{3n+1}$, n = 1, 2, and 3); (d) Quadruple-type perovskite ($AA'_3B_4O_{12}$) [49]

Double perovskite-structured materials have been attracting great attention recently as potential electrodes for electrochemical water splitting. Double perovskites have been known to exhibit physiochemical properties such as being able to lodge high valence elements for instance +6 or +7 in their structure, making them more tunable to suit the needs of an electrocatalyst for water splitting[55]. They have also been proven to exhibit high chemical and mechanical stability under harsh catalytic environments, like highly reducing or oxidizing conditions, strong alkaline or acidic solutions, and high temperatures[56]–[60].

$LaFeO_3$ has shown to perform in electrocatalytic oxygen evolution reaction, indicating that it has a potential for improved performance is more Lanthanum deficiencies are introduced onto the A-site of the catalyst [61]. $BaTiO_{3-\delta}$ (=0.24) is

another example as it has demonstrated excellent performances of OER, even exceeding the performance of IrO_2 at low overpotentials [62]. Tang et al, synthesized and tested a perovskite compound $LaCo_{0.2}Fe_{0.8}O_{3-\delta}$ and reported favorable results of the sulfurized version of the material. An OER of 360 mV and an HER of 340 mV, both measured at 10 mA/cm^2 were reported in 1 M KOH. The material also proved to be stable for 500 cycles, as reported, for cyclic voltammetry [63].

Summary

In this chapter, the literature review of the study has been presented. The advantage of using hydrogen as a fuel has been discussed in detail along with the common hydrogen production techniques. Electrochemical water-splitting for the production of hydrogen has been discussed in detail with their reaction mechanisms. Common materials for water-splitting have been explored with advantages and limitations for each category of material.

References

[1] D.-D. Huang *et al.*, "In situ synthesis of a Fe_3S_4/MIL-53 (Fe) hybrid catalyst for an efficient electrocatalytic hydrogen evolution reaction," *Chem. Commun.*, vol. 55, no. 31, pp. 4570–4573, 2019.

[2] S. Roy *et al.*, "Electrocatalytic Hydrogen Evolution from a Cobaloxime-Based Metal–Organic Framework Thin Film," *J. Am. Chem. Soc.*, vol. 141, no. 40, pp. 15942–15950, 2019.

[3] I. Dincer, "Green methods for hydrogen production," *Int. J. Hydrogen Energy*, vol. 37, no. 2, pp. 1954–1971, 2012.

[4] M. A. DeLuchi, "Hydrogen vehicles: an evaluation of fuel storage, performance, safety, environmental impacts, and cost," *Int. J. Hydrogen Energy*, vol. 14, no. 2, pp. 81–130, 1989.

[5] M. Momirlan *et al.*, "The properties of hydrogen as fuel tomorrow in sustainable energy system for a cleaner planet," *Int. J. Hydrogen Energy*, vol. 30, no. 7, pp. 795–802, 2005.

[6] M. Momirlan *et al.*, "Current status of hydrogen energy," *Renew. Sustain. energy Rev.*, vol. 6, no. 1–2, pp. 141–179, 2002.

[7] J. Hord, "Hydrogen safety: an annotated bibliography of regulations, standards and guidelines," *Int. J. Hydrogen Energy*, vol. 5, no. 6, pp. 579–584, 1980.

[8] L. Zhou, "Progress and problems in hydrogen storage methods," *Renew. Sustain. Energy Rev.*, vol. 9, no. 4, pp. 395–408, 2005.

[9] H. J. Pasman *et al.*, "Safety challenges in view of the upcoming hydrogen economy: An overview," *J. Loss Prev. Process Ind.*, vol. 23, no. 6, pp. 697–704, 2010.

[10] D. Das *et al.*, "Advances in biological hydrogen production processes," *Int. J. Hydrogen Energy*, vol. 33, no. 21, pp. 6046–6057, 2008.

[11] J. Zheng *et al.*, "Development of high pressure gaseous hydrogen storage technologies," *Int. J. Hydrogen Energy*, vol. 37, no. 1, pp. 1048–1057, 2012.

[12] A. Züttel, "Materials for hydrogen storage," *Mater. today*, vol. 6, no. 9, pp. 24–33, 2003.

[13] B. Sakintuna *et al.*, "Metal hydride materials for solid hydrogen storage: a review," *Int. J. Hydrogen Energy*, vol. 32, no. 9, pp. 1121–1140, 2007.

[14] P. Nikolaidis *et al.*, "A comparative overview of hydrogen production

processes," *Renew. Sustain. Energy Rev.*, vol. 67, pp. 597–611, 2017, doi: https://doi.org/10.1016/j.rser.2016.09.044.

[15] A. Richel, "Blue, green, gray: the colors of hydrogen." http://www.chem4us.be/blue-green-gray-the-colors-of-hydrogen/.

[16] S. Patial *et al.*, "Tunable photocatalytic activity of $SrTiO_3$ for water splitting: Strategies and future scenario," *J. Environ. Chem. Eng.*, 2020, doi: 10.1016/j.jece.2020.103791.

[17] H. M. El-Bery *et al.*, "Photocatalytic hydrogen generation via water splitting using ZIF-67 derived Co_3O_4@C/TiO_2," *J. Environ. Chem. Eng.*, 2021, doi: 10.1016/j.jece.2021.105702.

[18] A. Richel, "Blue, green, gray: the colors of hydrogen," 2021. http://www.chem4us.be/blue-green-gray-the-colors-of-hydrogen/.

[19] IEA, "The Future of Hydrogen," *Futur. Hydrog.*, 2019.

[20] J. Yin *et al.*, "Optimized metal chalcogenides for boosting water splitting," *Adv. Sci.*, vol. 7, no. 10, p. 1903070, 2020.

[21] C. G. Morales-Guio *et al.*, "Nanostructured hydrotreating catalysts for electrochemical hydrogen evolution," *Chemical Society Reviews*. 2014, doi: 10.1039/c3cs60468c.

[22] Y. Li *et al.*, "MoS_2 nanoparticles grown on graphene: An advanced catalyst for the hydrogen evolution reaction," *J. Am. Chem. Soc.*, 2011, doi: 10.1021/ja201269b.

[23] B. You *et al.*, "Enhancing electrocatalytic water splitting by strain engineering," *Adv. Mater.*, vol. 31, no. 17, p. 1807001, 2019.

[24] J. Zhang *et al.*, "Support and interface effects in water-splitting electrocatalysts," *Adv. Mater.*, vol. 31, no. 31, p. 1808167, 2019.

[25] H. Sun *et al.*, "Self-supported transition-metal-based electrocatalysts for hydrogen and oxygen evolution," *Adv. Mater.*, vol. 32, no. 3, p. 1806326, 2020.

[26] J. Yu *et al.*, "Recent advances and prospective in ruthenium-based materials for electrochemical water splitting," *Acs Catal.*, vol. 9, no. 11, pp. 9973–10011, 2019.

[27] D. W. Lima *et al.*, "PtNi and PtMo nanoparticles as efficient catalysts using TEA-PS.BF_4 ionic liquid as electrolyte towards HER," *Int. J. Hydrogen*

Energy, 2017, doi: 10.1016/j.ijhydene.2016.11.166.

[28] X. Cheng *et al.*, "Highly active, stable oxidized platinum clusters as electrocatalysts for the hydrogen evolution reaction," *Energy Environ. Sci.*, 2017, doi: 10.1039/c7ee02537h.

[29] J.-W. Tian *et al.*, "A new 2D Co_5-cluster based MOF: Crystal structure, magnetic properties and electrocatalytic hydrogen evolution reaction," *Inorg. Chem. Commun.*, vol. 95, pp. 73–77, 2018.

[30] Y. Li *et al.*, "Recent advances on water-splitting electrocatalysis mediated by noble-metal-based nanostructured materials," *Adv. Energy Mater.*, vol. 10, no. 11, p. 1903120, 2020.

[31] M. H. Miles *et al.*, "Periodic Variations of Overvoltages for Water Electrolysis in Acid Solutions from Cyclic Voltammetric Studies," *J. Electrochem. Soc.*, 1976, doi: 10.1149/1.2132619.

[32] S. Hu *et al.*, "Ni_3N/NF as Bifunctional Catalysts for Both Hydrogen Generation and Urea Decomposition," *ACS Appl. Mater. Interfaces*, 2019, doi: 10.1021/acsami.8b19052.

[33] W. Zhao *et al.*, "Novel Cobalt-Doped $Ni_{0.85}Se$ Chalcogenides ($Co_xNi_{0.85-x}Se$) as High Active and Stable Electrocatalysts for Hydrogen Evolution Reaction in Electrolysis Water Splitting," *ACS Appl. Mater. Interfaces*, 2018, doi: 10.1021/acsami.8b12797.

[34] K. Zhang *et al.*, "Molybdenum selenide electrocatalysts for electrochemical hydrogen evolution reaction," *ChemElectroChem*, vol. 6, no. 14, pp. 3530–3548, 2019.

[35] X. Xu *et al.*, "A perovskite electrocatalyst for efficient hydrogen evolution reaction," *Adv. Mater.*, vol. 28, no. 30, pp. 6442–6448, 2016.

[36] F. Song *et al.*, "Transition metal oxides as electrocatalysts for the oxygen evolution reaction in alkaline solutions: an application-inspired renaissance," *J. Am. Chem. Soc.*, vol. 140, no. 25, pp. 7748–7759, 2018.

[37] Y. Shi *et al.*, "Recent advances in transition metal phosphide nanomaterials: synthesis and applications in hydrogen evolution reaction," *Chem. Soc. Rev.*, vol. 45, no. 6, pp. 1529–1541, 2016.

[38] I. Katsounaros *et al.*, "Oxygen electrochemistry as a cornerstone for sustainable energy conversion," *Angew. Chemie Int. Ed.*, vol. 53, no. 1, pp.

102–121, 2014.

[39] S. Anantharaj *et al.*, “Amorphous Catalysts and Electrochemical Water Splitting: An Untold Story of Harmony,” *Small*. 2020, doi: 10.1002/smll.201905779.

[40] P. Chen *et al.*, “Recent progress of transition metal carbides/nitrides for electrocatalytic water splitting,” *J. Alloys Compd.*, vol. 883, p. 160833, 2021, doi: https://doi.org/10.1016/j.jallcom.2021.160833.

[41] X. Peng *et al.*, “Recent advance and prospectives of electrocatalysts based on transition metal selenides for efficient water splitting,” *Nano Energy*, vol. 78, p. 105234, 2020, doi: https://doi.org/10.1016/j.nanoen.2020.105234.

[42] M. Yang *et al.*, “Advances and Challenges of Fe-MOFs Based Materials as Electrocatalysts for Water Splitting,” *Appl. Mater. Today*, vol. 20, p. 100692, 2020, doi: https://doi.org/10.1016/j.apmt.2020.100692.

[43] B.-Q. Li *et al.*, “An aqueous preoxidation method for monolithic perovskite electrocatalysts with enhanced water oxidation performance,” *Sci. Adv.*, vol. 2, no. 10, p. e1600495, 2016.

[44] J. H. Montoya *et al.*, “Trends in adsorption of electrocatalytic water splitting intermediates on cubic ABO_3 oxides,” *Phys. Chem. Chem. Phys.*, vol. 20, no. 5, pp. 3813–3818, 2018.

[45] J. Xu *et al.*, “Recent advances in oxygen electrocatalysts based on perovskite oxides,” *Nanomaterials*, vol. 9, no. 8, p. 1161, 2019.

[46] S. Liu *et al.*, “Structure-engineered electrocatalyst enables highly active and stable oxygen evolution reaction over layered perovskite $LaSr_3Co_{1.5}Fe_{1.5}O_{10-\delta}$,” *Nano Energy*, vol. 40, pp. 115–121, 2017.

[47] S. Yagi *et al.*, “Covalency-reinforced oxygen evolution reaction catalyst,” *Nat. Commun.*, vol. 6, no. 1, pp. 1–6, 2015.

[48] J. Wang *et al.*, “Water splitting with an enhanced bifunctional double perovskite,” *ACS Catal.*, vol. 8, no. 1, pp. 364–371, 2018.

[49] D. Lee *et al.*, “Controlling oxygen mobility in Ruddlesden–Popper oxides,” *Materials (Basel).*, vol. 10, no. 4, p. 368, 2017.

[50] F. Calle-Vallejo *et al.*, “Number of outer electrons as descriptor for adsorption processes on transition metals and their oxides,” *Chem. Sci.*, vol. 4, no. 3, pp. 1245–1249, 2013.

[51] K. Lam *et al.*, "H_2O_2 treated $La_{0.8}Sr_{0.2}CoO_{3-\delta}$ as an efficient catalyst for oxygen evolution reaction," *Electrochim. Acta*, vol. 244, pp. 139–145, 2017.

[52] X. Du *et al.*, "PLD-fabricated perovskite oxide nanofilm as efficient electrocatalyst with highly enhanced water oxidation performance," *Appl. Catal. B Environ.*, vol. 272, p. 119046, 2020.

[53] Q. Sun *et al.*, "Double perovskite $PrBaCo_2O_{5.5}$: An efficient and stable electrocatalyst for hydrogen evolution reaction," *J. Power Sources*, vol. 427, pp. 194–200, 2019.

[54] Y. Bu *et al.*, "A composite catalyst based on perovskites for overall water splitting in alkaline conditions," *ChemElectroChem*, vol. 6, no. 5, pp. 1520–1524, 2019.

[55] S. Vasala *et al.*, "$A_2B'B''O_6$ perovskites: A review," *Progress in Solid State Chemistry*. 2015, doi: 10.1016/j.progsolidstchem.2014.08.001.

[56] T. Shinagawa *et al.*, "Effect of reverse Boudouard reaction catalyst on the performance of solid oxide carbon fuel cells integrated with a dry gasifier," *Adv. Mater.*, vol. 31, no. 11, p. 1903070, 2019, doi: https://doi.org/10.1016/j.ijhydene.2018.04.200.

[57] S. Sengodan *et al.*, "Layered oxygen-deficient double perovskite as an efficient and stable anode for direct hydrocarbon solid oxide fuel cells," *Nat. Mater.*, 2015, doi: 10.1038/nmat4166.

[58] S. Geiger *et al.*, "The stability number as a metric for electrocatalyst stability benchmarking," *Nat. Catal.*, 2018, doi: 10.1038/s41929-018-0085-6.

[59] A. Grimaud *et al.*, "Double perovskites as a family of highly active catalysts for oxygen evolution in alkaline solution," *Nat. Commun.*, 2013, doi: 10.1038/ncomms3439.

[60] L. Zhou *et al.*, "Synthesis and Photocatalytic Application of Stable Lead-Free $Cs_2AgBiBr_6$ Perovskite Nanocrystals," *Small*, 2018, doi: 10.1002/smll.201703762.

[61] Y. Zhu *et al.*, "Enhancing electrocatalytic activity of perovskite oxides by tuning cation deficiency for oxygen reduction and evolution reactions," *Chem. Mater.*, vol. 28, no. 6, pp. 1691–1697, 2016.

[62] C.-F. Chen *et al.*, "Oxygen-deficient $BaTiO_{3-x}$ perovskite as an efficient bifunctional oxygen electrocatalyst," *Nano Energy*, vol. 13, pp. 423–432,

2015.

[63] L. Tang *et al.*, “Enhancing perovskite electrocatalysis through synergistic functionalization of B-site cation for efficient water splitting,” *Chem. Eng. J.*, 2020, doi: 10.1016/j.cej.2020.126082.

Chapter 3: Materials and Methods

3.1 Synthesis

Analytical-grade $Sr(NO_3)_2$ (98%, Alfa Aesar, UK), $C_{12}H_{28}O_4Ti$ / $Ti[OCH(CH_3)_2]_4$ (titanium isopropoxide [TTIP]) (97%, Sigma, USA), $Fe(NO_3)_3.9H_2O$ (98%, Alfa Aesar, Belgium), and $Pr(NO_3)_3.xH_2O$ (98%, Alfa Aesar, Belgium), were all used as metal precursors. For chelating agent and as the fuel for sol-gel combustion Glycine (99.7%, VWR chemicals, Belgium) was used.

Perovskite oxides have traditionally been synthesized using the ceramic technique or solid-state reaction, wherein oxides of precursor metals were combined and allowed to react at high temperatures. However, soft chemistry routes, such as sol-gel combustion, have been proved to be an adequate alternative route for acquiring perovskites. When contrasted to the ceramic method, soft chemistry materials have higher porosity and substantially smaller particle size, and also better stoichiometric regulation and reduced synthesis temperatures [1]. An extensive assortment of perovskite oxides have been produced utilizing variants of the Pechini method or the sol-gel combustion method [2], [3]. The Pechini technique requires the use of a -hydroxycarboxylic organic acid, such as citric acid or α-amino acid capable of forming stable chelates with multiple cations at the same time, such as glycine. These acids serve as a chelating agent and a fuel for self-combustion. This method is beneficial since it uses less costly precursors to form a complex of cations in an aqueous medium, culminating in a molecularly uniform ion distribution. The solution is heated after the chelating agent has been dissolved with precursor salts, converting the chelate into a polymer with evenly distributed cations. The organic component is removed from the solution by self-combustion at temperatures as low as 300 °C [1].

$Sr_2TiFeO_{6-\delta}$ (STF) and Pr-doped STF were synthesized using the Pechini method. Fig. 3-1 illustrates the schematic flow of the synthesis of the electrocatalysts. The precursor solution was made by dissolving metal nitrates salts in the stoichiometric amounts of Sr, and Fe (2:1, respectively) in deionized water while ethanol was used as a solvent to dissolve TTIP at room temperature. Both the solutions were stirred separately for 3 hours and were then mixed. Afterward, glycine

powder was added into the solution obtained by combining the two solutions (Sr and Fe salts dissolved in water and TTIP dissolved in ethanol). Using the propellant chemistry principles, the stoichiometric amount of glycine required was calculated using the valences of reducing and oxidizing elements. The optimal stoichiometric glycine to metal cation ratio required to obtain STF powder is 2:1 [4].

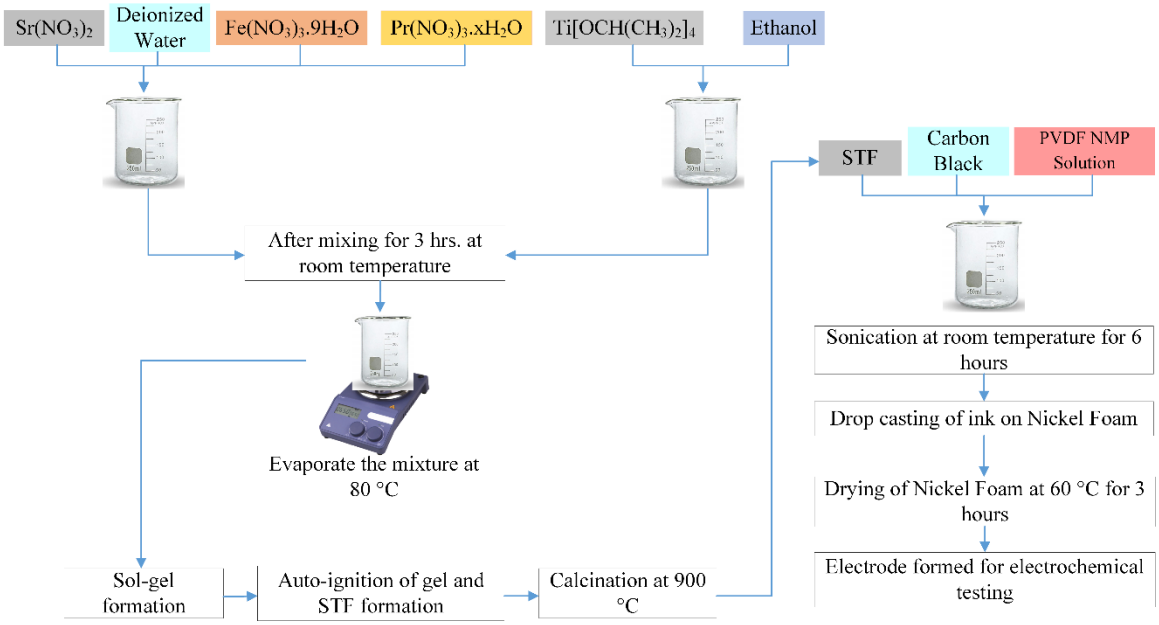

Figure 3-1 – Schematic of electrocatalyst synthesis

The mixture of the two solutions was evaporated using a hot plate while it was stirred continuously at 90°C until a viscous gel was obtained. The hotplate temperature was then increased to 300°C which resulted in auto-ignition of the gel and formation of black STF ash. The self-combusted gel was then dried overnight at 120°C for 12 hours in a preheated oven. The dried black ash was then calcined at 900°C for 3 hours in the air (Magma Therm, Model: CWF1200, Turkey) to obtain pure black double perovskite STF powder. Similarly, praseodymium was doped at A and B-site of STF to obtain $Sr_{1.9}Pr_{0.1}TiFeO_{6-\delta}$, $Sr_{1.8}Pr_{0.2}TiFeO_{6-\delta}$, $SrTiFe_{0.9}Pr_{0.1}O_{6-\delta}$, and $SrTiFe_{0.8}Pr_{0.2}O_{6-\delta}$ which were identified as SPTF01, SPTF02, STFP01, and STFP02, respectively.

3.2 Catalyst Characterization and Techniques Overview

Table 3-1 Details of characterizations techniques used in this study

Characterization	Information Extracted	Process Parameters	Equipment

Technique			Make/Model
TGA	Thermal stability	• Window = 20°C to 900°C • Ramp = 10°C/min Atmosphere = N_2 gas (50 mL/min)	Shimadzu, DTG-60H
XRD	Phase characterization	• $2\theta = 10° - 80°$ • Scan rate = $0.2°s^{-1}$ • CuKα radiation (λ = 0.15418 nm)	D8-Advance, Bruker
SEM	Surface morphology	Operating voltage = 20kV	TESCAN MIRA3 LMU
EDS	Elemental composition and mapping	Operating voltage = 20kV	Oxford instruments INCAx-act, model 51-ADD0007
N_2 adsorption-desorption	• Pore volume (BJH method) • Pore diameter (BJH method) • Specific surface area (single point technique)	• Degassing at 150°C for 6 hours • Isotherms were obtained at −196°C	Quantachrome NovaWin

3.2.1 Thermogravimetric Analysis (TGA)

TGA, or thermogravimetric analysis, is a thermoanalytical method used to identify the thermostability of a specimen or material. The sample is heated at a steady rate in TGA, and its weight change is monitored closely. The graph acquired temperature as well as mass percentage are used to determine the ratio of volatile components present. As a consequence, TGA can be used to characterize materials that go through mass changes, whether loss or gain, as a result of decomposition, dehydration, and oxidation [5]. TGA can be performed in any environment needed for the analysis; for example, if the analysis is required in an inert atmosphere, Nitrogen gas is used.

The TGA unit comprises of a super sensitive scale capable of monitoring weight in fractions of a milligramme, that is used to quantify the weight change as

the sample is heated in a thermally secluded compartment in a controlled fashion by a programable furnace. Thermal isolation of the balance enhances the precision, sensitivity, and accuracy of mass measurements [6].

3.2.2 X-Ray Diffraction (XRD)

XRD is used to investigate a substance's crystal structure using X-rays since their wavelength is of the same order as the distance between atoms within a material's crystal structure and can be used to obtain the mean distance between the layers or atomic rows within the crystal. The technique is used to estimate the size and shape of crystallites, and even the grain or single-crystal alignment [7]. A beam of X-rays is aimed on to crystalline material to be investigated, which then disperses these X-rays elastically due to the lattice's periodic nature. Dispersion of X-rays happen as a consequence of interplay between X-ray photons and atom outermost shell electrons [8].

When X-rays are irradiated on a crystalline structure, the X-rays are dispersed, allowing constructive and destructive intrusion of the X-ray beam, culminating in a diffraction pattern that is distinctive to that crystalline material, equivalent to a fingerprint. The generated diffractogram has many sharp peaks, also known as Bragg diffraction peaks. For a crystalline specimen, the XRD diffractogram reveals sharp peaks at specific angles, while for an amorphous sample, the maximum intensity expands over several degrees [8]. Bragg's law describes the distance between atoms and their interplay with the wavelength of irradiated X-rays, which results in diffraction:

$$2dsin\theta = n\lambda$$

where d denotes the perpendicular distance between two adjacent atomic planes, θ is the incidence angle of X-rays at which diffraction takes place, λ is the wavelength of the irradiating X-ray beam, and *n* denotes an integer that signifies the order of reflection, which signifies the path difference between scattered waves from adjacent atomic planes [7].

XRD can also be used to estimate average crystallite size using the Scherrer equation and the widening of diffraction peaks:

$$t = K\lambda/\beta cos\theta$$

where t is the crystallite size, K is the Scherrer constant, λ is the wavelength of the irradiating X-ray beam, β and is the FWHM (full width at half maximum of the diffraction peak). However, the Scherrer equation doesn't quite compensate for intrinsic crystallite defects and strains, that can produce peak broadening. As a result, the crystallite size determined by XRD should not be regarded absolute and should be substantiated using other methods such as TEM [7], [8].

Finally, XRD can be used to evaluate the elemental make-up of a mixture, the variance of a specific crystalline material from its optimum structure and composition, and the material's crystallinity [9].

3.2.3 Scanning Electron Microscopy (SEM)

SEM, or scanning electron microscopy, is a method that uses a highly focused beam of electrons to generate high resolution images of a material's surface with a resolution of up to 1nm [10]. The electron beam interacts with the sample surface, producing characteristic X-rays as well as three types of signals: primary electrons elastically backscattered by the sample, secondary electrons inelastically backscattered by the sample, and Auger electrons. Secondary electrons or inelastically backscattered electrons can be used to develop high resolution images of the specimen surface. The distinctive X-rays are used to identify the elements present in the sample by using energy dispersive X-ray analysis (EDX) technique, whereas the Auger electrons are used in surface analysis techniques [7], [9].

The sample must be electrically conductive for SEM because electrostatic charge will accumulate on its surface unless the sample is not conductive and/or correctly grounded, resulting in distorted images. Non-conductive samples are thus coated with an extremely fine layer of gold to make them conductive. The sample also must be free of water content, as SEM vaporizes under high vacuum conditions, causing water to evaporate and inhibiting image clarity [8].

3.2.4 N_2 Adsorption – Desorption

The surface area of a material is measured using N_2 adsorption – desorption. Adsorption occurs when N_2 is physically adsorbed on the surface of a sample at low

temperatures, whereas desorption occurs when N_2 breaks away from the surface of a sample at high temperatures. The adsorbed N_2 can form a monomolecular or multimolecular layer on the sample's surface. Because adsorption is physical in nature, this is not selective, i.e., N_2 would then adsorb upon this surface of any sample at its boiling point [11].

Typically, the Brunauer-Emmett-Teller model is used to assess the surface area of a sample based on the adsorption – desorption isotherms acquired. After reaching equilibrium during analysis, the quantity of N_2 adsorbed can be determined by adjusting the pressure of N_2. Such calculations are replicated at multiple N_2 pressures to obtain an adsorption isotherm, which can be used to determine pore size and pore volume distribution, as well as the sample's surface area. The Barrett-Joyner-Halenda (BJH) model is commonly used to estimate pore size and pore volume distribution [12].

3.3 Experimental Setup for Electrochemical Measurements

Electrochemical measurements were carried out on an Electrochemical workstation (Model 660E by CH Instruments) equipped with a three-electrode assembly. The reference and counter electrodes of Ag/AgCl and Platinum wire were used, while nickel foam-based working electrode was used in the setup.

The working electrodes for the three-electrode assembly were nickel foam-based electrodes, while the reference and counter electrodes were Ag/AgCl and Pt. wire, respectively. Firstly, the nickel foam substrate was treated by sonication in 3 M HCl, distilled water, and ethanol respectively, for 15 mins individually. The Ni foam pieces were then dried at 60°C for 2 hours. Finally, the ink was prepared by mixing 15 mg of active material, 3 mg of carbon black, and 2 mg of PVDF in 100 µL of NMP. The solution was sonicated overnight to ensure thorough dispersion. The ink was drop casted onto the nickel foam of 1x1 cm^2 and was left to be dried at 60°C for 3 hours. The electrochemical measurements of all electrocatalyst have been analyzed in 2 M KOH solution at varying scan rates. Oxygen evolution reaction (OER), hydrogen evolution reaction (HER), cyclic voltammetry (CV), and impedance spectroscopy (EIS) were the tests carried out for each sample. Reversible hydrogen

electrode (RHE) potential was used for further calculations. The following equation was used to obtain the values of RHE potential with the pH of 14 [13]:

$$E_{RHE} = E_{Ag/AgCl} + 0.059pH + 0.1976$$

For 2-electode assembly, the working and the counter electrodes were both nickel foam based. The fabrication technique for 2-electrode was same as the one discussed above for 3-electrode assembly. The LSV was performed for the 2-electrode assembly for overall water splitting from 1-2 V for the electrolyzers.

Summary

In this chapter, the synthesis route used for sample preparation has been discussed. The characterization techniques used to determine the physical and chemical properties of the material has been discussed in detail. The instruments used and their respective parameters has been listed, along with the equations used for calculations.

References

[1] A. M. Huízar-Félix *et al.*, "Sol-gel based Pechini method synthesis and characterization of $Sm_{1-x}Ca_xFeO_3$ perovskite $0.1 \leq x \leq 0.5$," *Powder Technol.*, 2012, doi: 10.1016/j.powtec.2012.06.057.

[2] P. Hao *et al.*, "Sol–gel combustion synthesis and antiferromagnetic properties of orthorhombic perovskite-type $MFeO_3:R^{3+}$ (M=La, Gd; R=Eu, Er, Ho) nanocrystalline powders," *J. Solid State Chem.*, 2020, doi: 10.1016/j.jssc.2019.121087.

[3] M. Dara *et al.*, "Green sol-gel auto combustion synthesis and characterization of double perovskite Tb_2ZnMnO_6 nanoparticles and a brief study of photocatalytic activity," *RSC Adv.*, 2021, doi: 10.1039/d0ra10400k.

[4] U. M. Khan *et al.*, "Synthesis of cobalt loaded double perovskite $Sr_2TiFeO_{6-\delta}$ (STF) as a stable catalyst for enhanced hydrogen production via methane decomposition," *Int. J. Energy Res.*, 2021, doi: 10.1002/er.7084.

[5] K. Hildal *et al.*, "Metals and Alloys," in *Handbook of Thermal Analysis and Calorimetry*, vol. 6, Elsevier, 2018, pp. 781–828.

[6] S. Ebnesajjad, "Introduction to fluoropolymers," in *Applied Plastics Engineering Handbook*, Elsevier, 2017, pp. 55–71.

[7] P. H. Salame *et al.*, "Characterization tools and techniques for nanomaterials," in *Nanomaterials for green energy*, Elsevier, 2018, pp. 83–111.

[8] M. Kaliva *et al.*, "Nanomaterials characterization," in *Polymer Science and Nanotechnology*, Elsevier, 2020, pp. 401–433.

[9] D. Titus *et al.*, "Nanoparticle characterization techniques," in *Green synthesis, characterization and applications of nanoparticles*, Elsevier, 2019, pp. 303–319.

[10] R. A. Shanks, "Characterization of nanostructured materials," in *Nanostructured Polymer Blends*, Elsevier, 2014, pp. 15–31.

[11] H.-J. Butt *et al.*, *Physics and chemistry of interfaces*. John Wiley & Sons, 2013.

[12] S. Yurdakal *et al.*, "Chapter 4 - (Photo)catalyst Characterization Techniques: Adsorption Isotherms and BET, SEM, FTIR, UV–Vis, Photoluminescence, and Electrochemical Characterizations," in *Heterogeneous Photocatalysis - Relationships with Heterogeneous Catalysis and Perspectives*, 1st ed., G.

Marcì and L.B.T.-H.P.Palmisano, Eds. Netherlands: Elsevier, 2019, pp. 87–152.

[13] R. Khan *et al.*, "3D hierarchical heterostructured LSTN@NiMn-layered double hydroxide as a bifunctional water splitting electrocatalyst for hydrogen production," *Fuel*, 2021, doi: 10.1016/j.fuel.2020.119174.

Chapter 4: Results and Discussion

4.1 Physicochemical Properties of the Electrocatalyst

Fig. 4-1(a) shows the TGA curve for uncalcined STF and the weight loss can be observed in two stages. The first phase of weight loss till around 300-400 °C for STF can be attributed to the moisture and carbon species. The second phase of weight loss (400-700 °C) for STF is due to the nitrates being evolved and the sudden weight loss around 800 °C can be attributed to the crystallization of STF. Fig. 4-1(b) shows the TGA curve of uncalcined SPTF01 and as can be seen that the weight loss for this is significantly higher than that of STF. The first phase of weight loss around 150-200 °C is due to moisture loss. The second phase in STFP01 (200-500 °C) is due to carbon species being lost, the weight loss around 500-600 °C is due to the evolution of nitrate species. Finally, the weight loss from 600-800 °C is due to the crystallization of STFP01. Praseodymium doping has been reported to cause significant weight losses in past studies [1], [2].

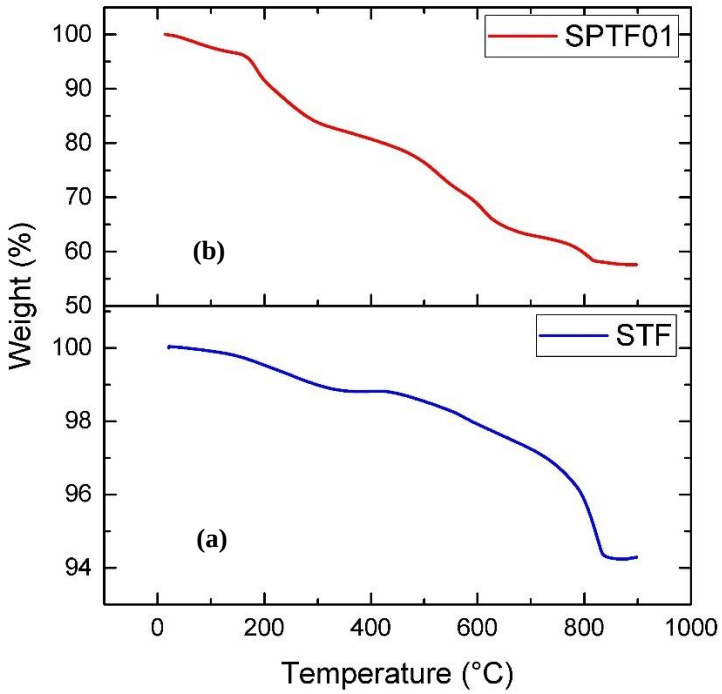

Figure 4-1 - TGA of uncalcined samples

Fig. 4-2 shows the XRD spectrograms of as calcined STF, STFP01, STFP02, SPTF01, and SPTF02. STF was identified as $Sr_2TiFeO_{5.5}$ with a cubic structure in the

pm-3m space group. Peak shifting was observed for both the A and B-site doped STF as can be seen in the inset image which shows the (110) peak (JCPDS # 38-1335). The A-site Pr-doped STF i.e., SPTF01 and SPTF02, only shows a shift in peak position which increases with the increase in the amount of Pr doping. Whereas no significant change in peak intensity was observed. Therefore, it can be concluded that Pr was successfully doped into the STF lattice, and it did not increase or decrease the crystallinity of STF. However, the B-site doping of Pr resulted in the formation of multiple impurity phases and a significant decrease in the crystallinity of doped STF as evident from the decrease in intensity of XRD spectra. The impurity phases detected were $SrPrFeO_4$ (JCPDS # 32-1237), TiO_2 (anatase) (JCPDS # 21-1272), and Fe_3O_4 (JCPDS # 390238). TiO_2 (anatase), and Fe_3O_4 were only detected for STFP01 and not for STFP02. The lattice parameters and crystallite sizes of the (110) peaks were calculated from the XRD Spectrogram and are presented in Table 4-1.

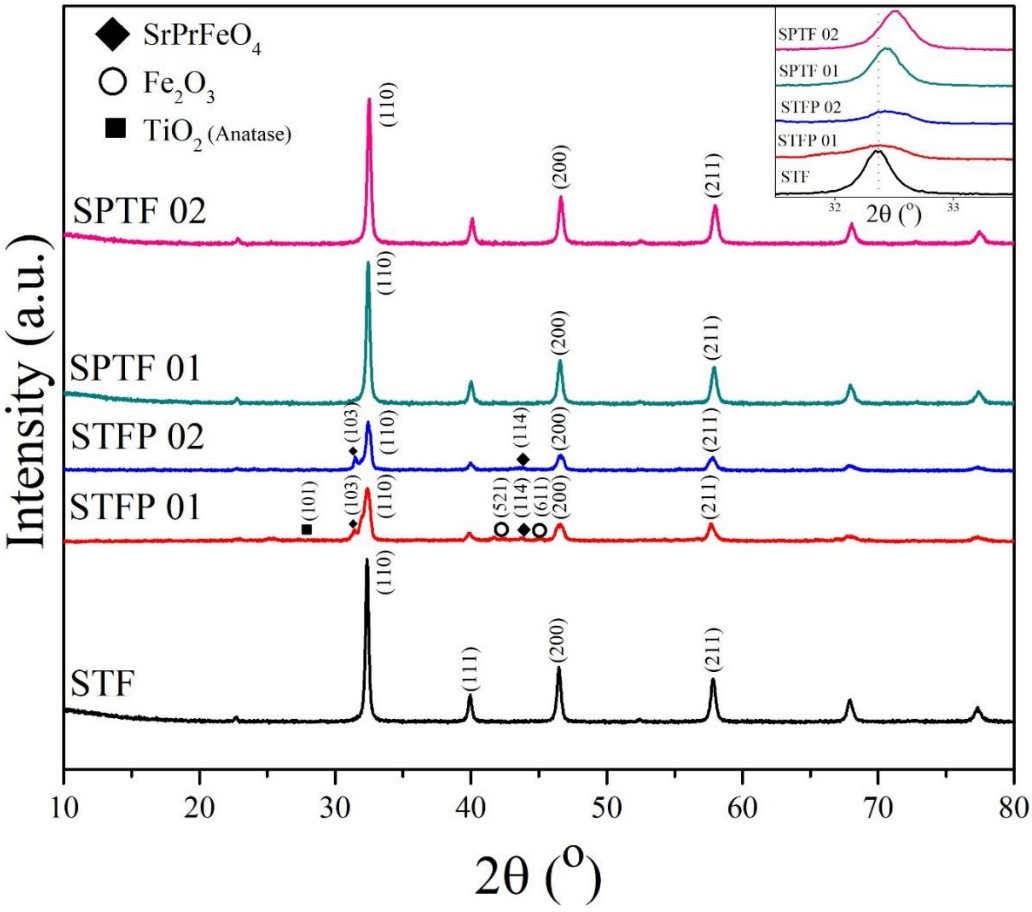

Figure 4-2 - XRD of as synthesized samples

Table 4-1 - Lattice Parameters of the synthesized electrocatalysts

Catalyst	2θ	Lattice Parameter (nm)	Crystallite Size (nm)
STF	22.8565	0.3912	0.4690
SPTF01	22.7666	0.3902	0.4283
SPTF02	22.8076	0.3890	0.4202
STFP01	22.8560	0.3905	0.3217
STFP02	22.80453	0.3898	0.3381

Fig. 4-3 shows the SEM images of STF, SPTF01, SPTF02, and STFP02 at 5 μm magnifications and the FESEM micrographs of STFP01 at 5 μm and 1 μm magnifications. The best performing sample of this study was STFP01, as is further discussed in this paper, and to ascertain its sponge-like morphology, FESEM images were taken as can be seen in Fig. 4-3(e-f). The STF double perovskite can be seen to possess a highly porous, sponge-like morphology whereas SPTF02 does not depict a sponge-like morphology but is highly porous. The porous structure depicted by STF, and its variants are ideal for an electrocatalyst as the porous structure provides an increased available surface area to catalyze the reaction.

Fig. 4-4 shows the EDS spectra of STF and STFP01, and as can be seen from the image that Praseodymium was clearly present in the STFP01 catalyst. Furthermore, no impurities are observed in either of the EDS spectra.

N_2 adsorption-desorption isotherms of STF and STFP1 are plotted in Fig. 4-5. Both of the catalysts, STF and STFP1, shows type IV isotherm and H3-type hysteresis loops as per IUPAC classification. Both of the analyzed electrocatalysts exhibited narrow-necked and slit-shaped mesoporous pores. The hysteresis loop is due to capillary condensation which takes place in mesopores by increasing the relative pressure [3]. Larger hysteresis loop of STFP1 is because it has a higher surface area than STF as can be seen in Table 4-2.

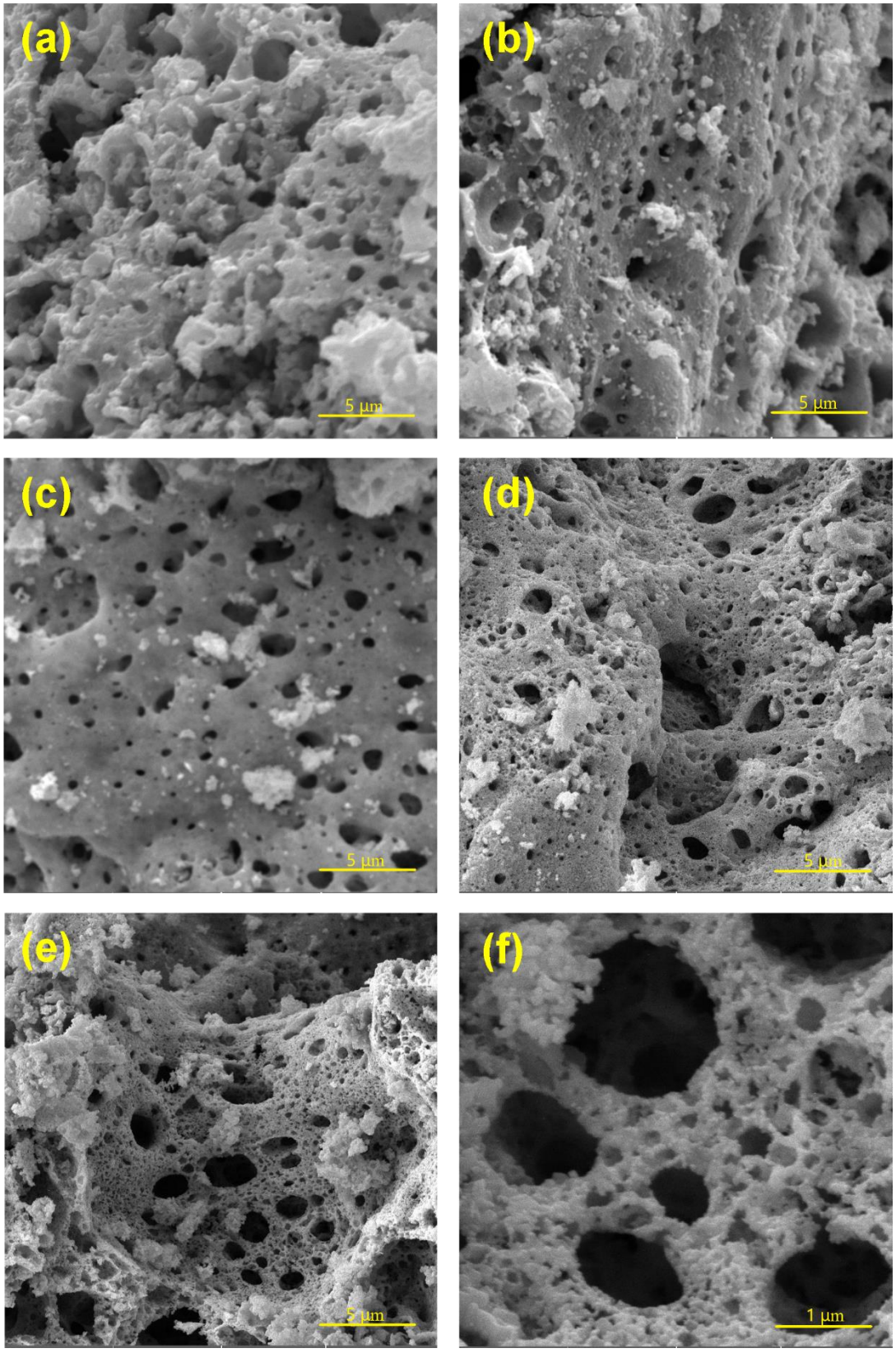

Figure 4-3 - SEM images of (a) STF at 5 µm (b) SPTF01 at 5 µm (c)SPTF02 at 5 µm (d) STFP02 at 5 µm (e)STFP01 at 5 µm (f) SPFT01 at 1 µm

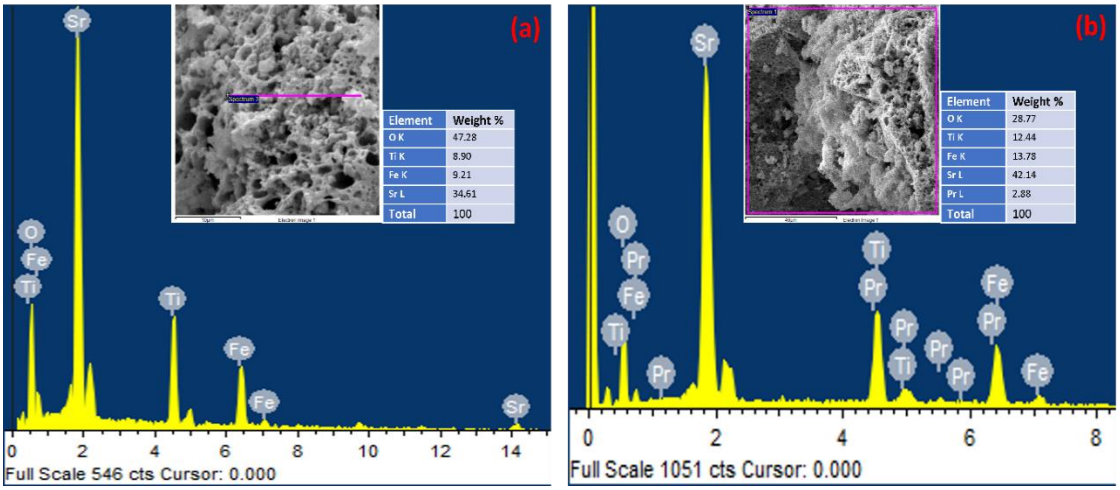

Figure 4-4 - EDS spectra of (a) STF (b) STFP01

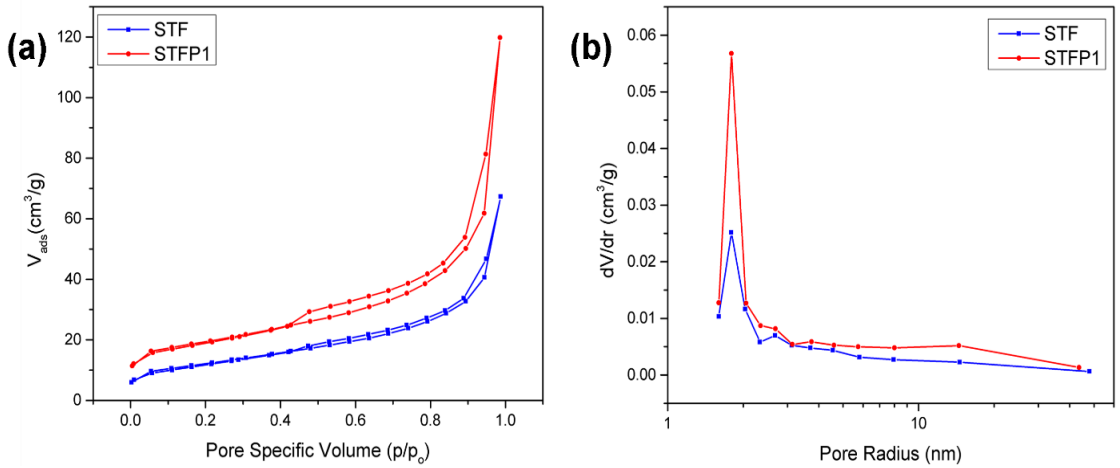

Figure 4-5 - (a) N_2 adsorption-desorption isotherm (b) BJH pore size distribution

Table 4-2 - N_2 Adsorption-Desorption Summary

Catalyst	Specific Surface Area (m^2/g)	BJH Adsorption Pore Volume (cm^3/g)	BJH Pore Diameter (nm)
STF	42.2849	0.009	3.246
STFP1	65.6362	0.014	3.242

4.2 Electrochemical Performance of Electrocatalysts

The OER performance of the prepared samples was determined through the LSV polarization curves. As can be seen from Fig. 4-6, STFP1 performs the best with the lowest overpotential of 277.6 mV, which is considerably lower than that of the base STF samples. This is further reinforced by the fact that STFP01 has the lowest slope of 73 mV/dec from the Taffel plots of all 5 samples. Furthermore, as nickel foam itself possesses a decent activity in OER, the measured electrocatalysts

have been compared to the performance of bare nickel foam as well in Fig. 4-6 (a) and (b).

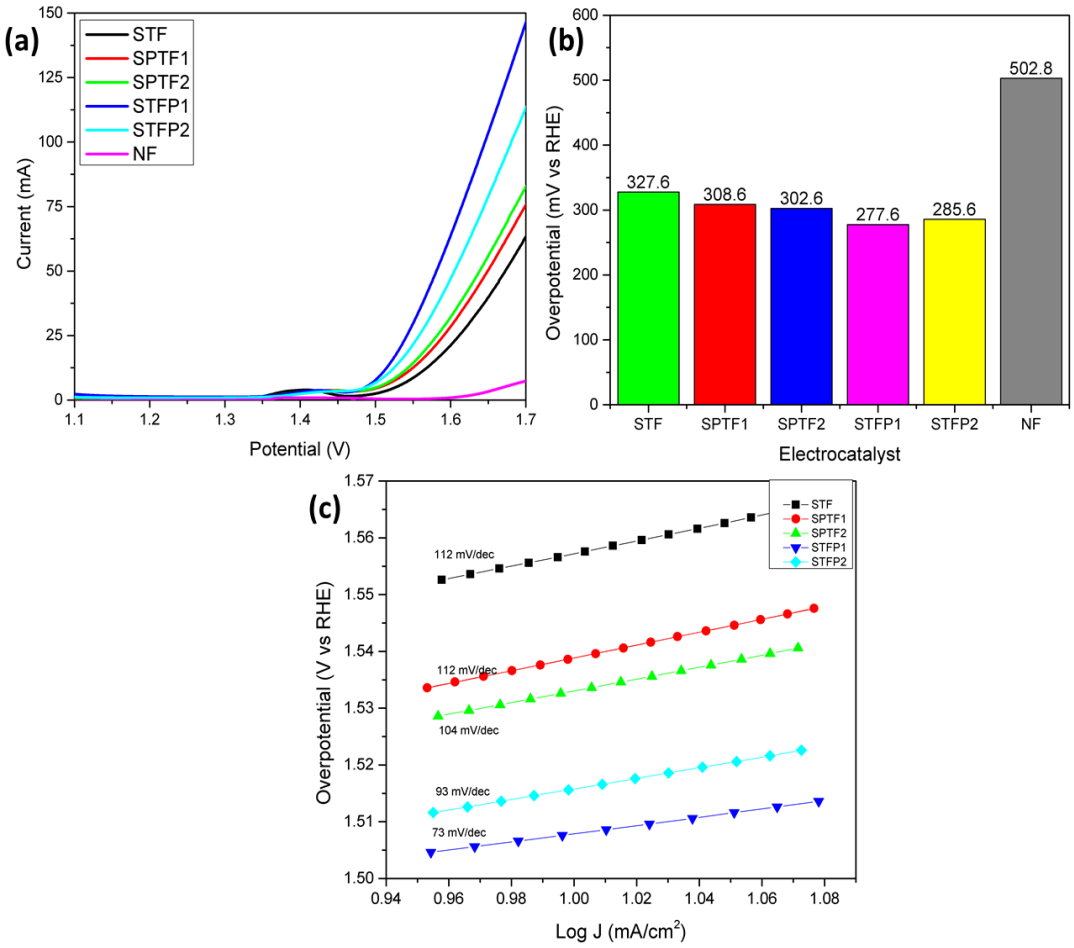

Figure 4-6 – (a) LSV curves for OER, (b) Overpotentials obtained for OER, (c) Taffel plots for OER

HERs for all 5 of the samples were again determined using the LSV polarization curves. And as can be seen in Fig. 4-7 that the sample STFP01 outperforms the rest of the samples with an overpotential of 182.4 mV and a Taffel plot slope of 77 mV/dec. Furthermore, as nickel foam itself possesses a decent activity in HER, the measured electrocatalysts have been compared to the performance of bare nickel foam as well in Fig. 4-7 (a) and (b). The mechanism of the reaction is given by the Volmer-Heyrovsky steps [4]:

Volmer step, electrochemical adsorption ≈ 120 mV/dec

$$H_2O + M + e^- \rightarrow M - H_{ads} + OH^-$$

Heyrovsky step, electrochemical desorption ≈ 40 mV/dec

$H_2O + M - H_{ads} + e^- \rightarrow H_2 + OH^-$

Tafel step, chemical desorption ≈ 30 mV/dec

$H_{ads} + H_{ads} \rightarrow H_2 + 2\ M$

Where M denotes active sites. The adsorbed hydrogen intermediate is generated in the alkaline solution when water molecules are discharged. The desorption process then results in the evolution of H_2 gas [5].

The overall decent electrochemical performance of doped STF can be attributed to its highly ordered double-perovskite structure. Furthermore, doping or Pr^{3+} into the STF structure can be seen to enhance the catalytic performance of the material in both OER and HER. A and B-site doping was studied to determine if it results in a change in performance. STFP01 performs better than the rest of the catalysts tested for this study, this can be attributed to the decreasing crystallinity in the STFP01 catalyst as compared to the rest of the catalysts studied in this research and it is evident from the XRD spectrograms in Fig.4-1. It has been concluded in recent publications that catalysts with less crystallinity tend to perform better as compared to more ordered crystal structures[6]. And that paired with the Ni foam further improves the performance of the catalysts, as the porous Ni foam support provides mechanical stability and aids in the transport of ions towards active sites [7]. A comparative performance of the catalysts tested in this study have been tabulated against recent publications in Table 4-4.

Fig. 4-8 (a) shows CV curves of all 5 samples taken at a scan rate of 5 mV/s. The potential range of 0-0.5 V shows clear redox peaks for all samples taken. The peaks for STF were at 0.374 V, 1.516 mA, and 0.271 V, -0.966 mA. The peaks for SPTF1 were at 0.401 V, 2.76 mA, and 0.275 V, -2.563 mA. The peaks for SPTF2 were at 0.362 V, 2.657 mA, and 0.282 V, -2.836 mA. The peaks for STFP1 were at 0.396 V, 3.039 mA, and 0.301 V, -3.784 mA. The peaks for STFP2 were at 0.408 V, 2.327 mA, and 0.292 V, -2.019 mA.

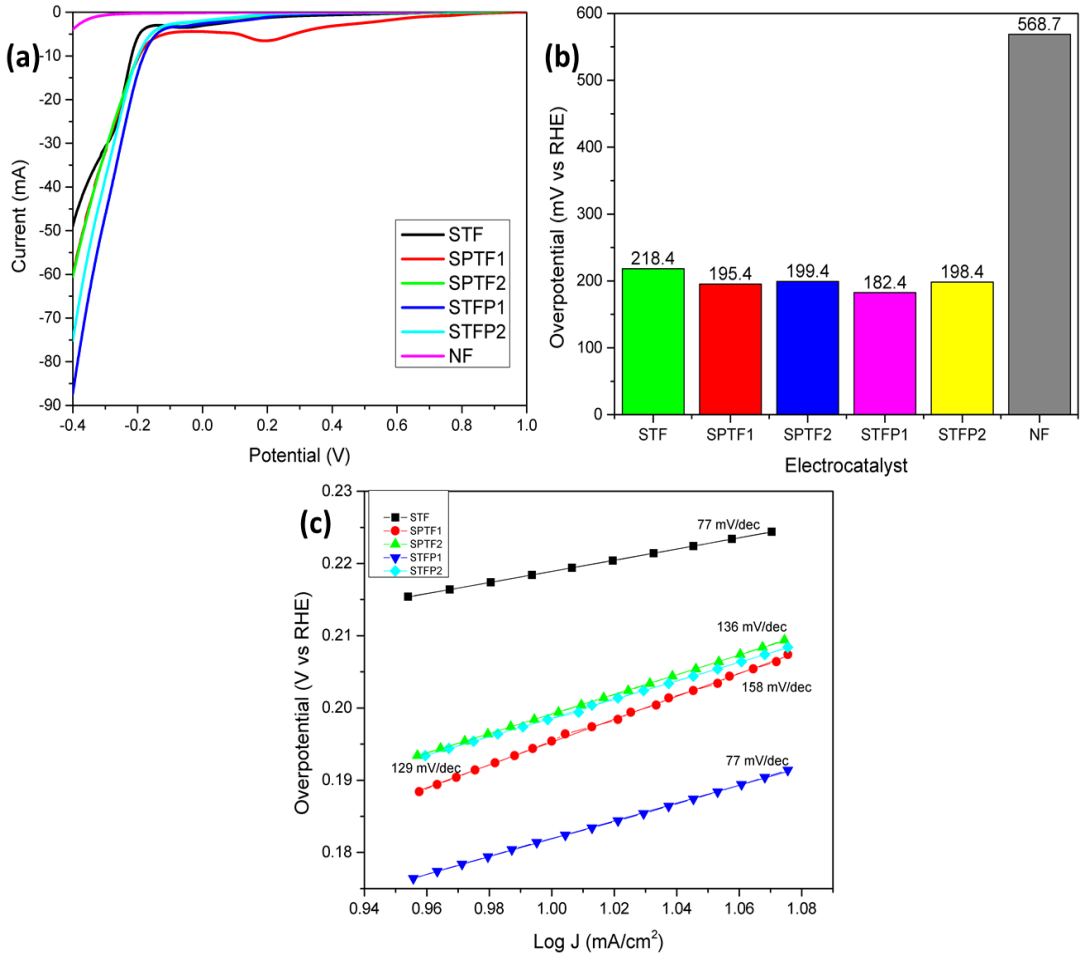

Figure 4-7 - (a) LSV curves for HER, (b) Overpotentials obtained for HER, (c) Taffel plots for HER

Electrochemical impedance spectroscopy measurements were used to investigate the kinetics of the synthesized electrocatalysts as shown in Fig. 4-8(b). The test was performed within a frequency range of 100 mHz to 1000 kHz at 10 mV. The graph inset shows equivalent circuit elements. R1 or RS represents the ohmic resistance of the electrolyte between the electrodes, the charge transfer resistance, given by R2 or RCT, represents the polarization resistance at the interface on the electrode and electrolyte, W is the Warburg impedance and C2 denotes the faradic capacitance. The resistances for each sample were calculated and have been tabulated in Table 4-3.

Stability is a very important factor for any electrocatalyst, as it helps determine the feasibility of a catalyst and its performance degradation over time. Fig. 4-8(c) shows the HER curves for the best performing sample before and after running the sample for 1000 cycles. The overpotential drops from 182.4 mV to 181.9 mV, which proves that the electrocatalyst is stable. The inset of Fig. 4-8(c) shows the

i-t curve for 12 h with a potential of 0.301 V as observed for the sample from the CV curves of STFP01. During this run the value of current drops from 0.543 mA to 0.0636 mA. Fig. 4-8(d) shows the stability of the OER performance of the sample STFP01 at 5 mV/s after 1000 cycles. The overpotential of OER increases from 277.6 mV to 280.5 after 1000 cycles, hence once again proving the stability of the catalyst.

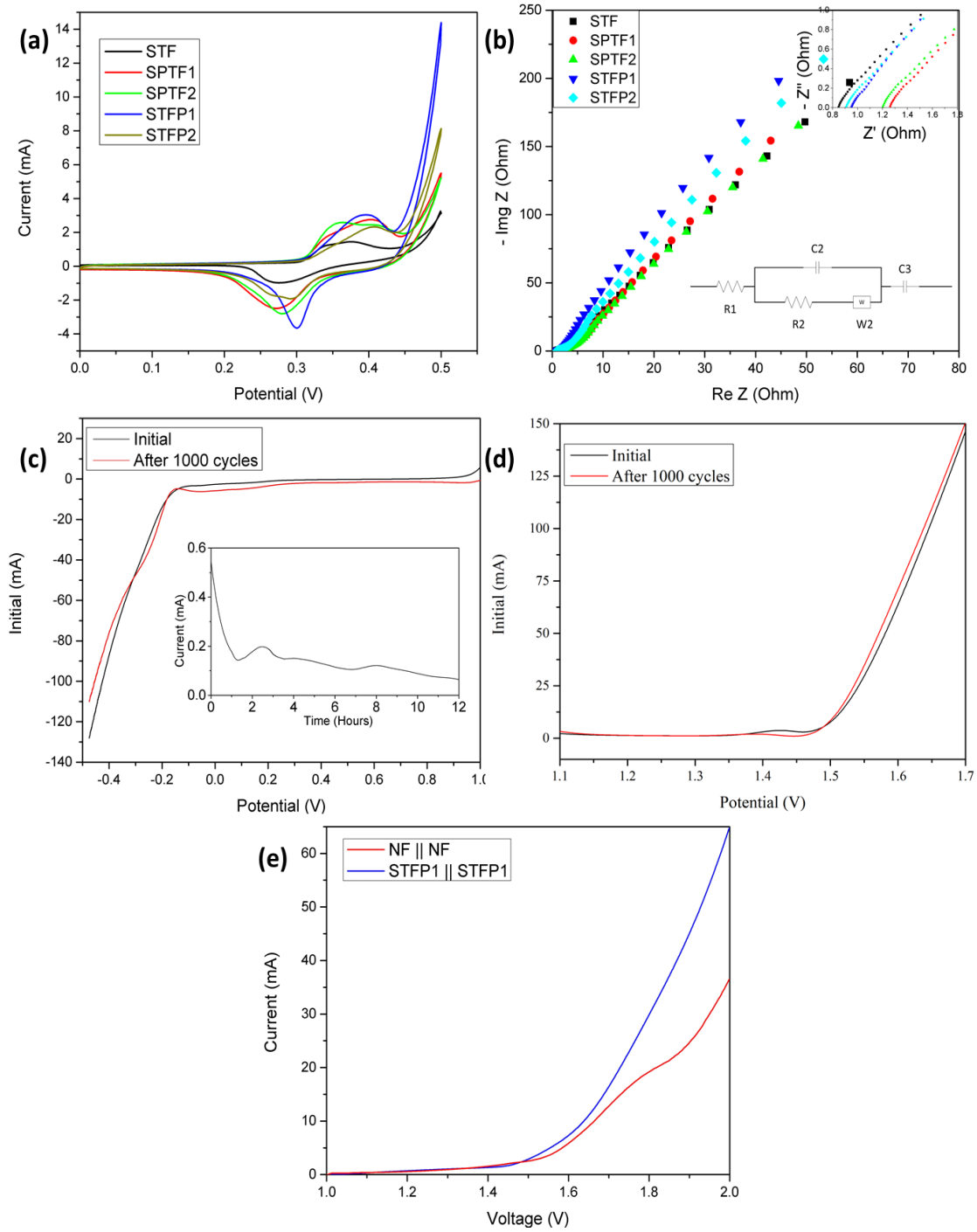

Figure 4-8 - (a) CV curves for all 5 samples (b) EIS for all samples (c) Stability test for HER at 5 mV/s for STFP01, inset shows i-t curve for 12 h (d) Stability test for OER at 5 mV/s fir STFP01 (e) Overall water splitting performance of NF || NF electrolyzer and STFP01 || STFP01 electrolyzer.

As the results discussed above indicate that the synthesized electrocatalysts depict excellent performance for both HER and OER, a device for the best performing sample was assembled to determine its overall water splitting performance. The NF || NF electrolyzer achieves the current of 10 mA at 1.665 V, compared to that the STFP01 || STFP01 electrolyzer achieved the same at only 1.638 V as can be seen in Fig. 4-8 (e).

As the results discussed above indicate that the synthesized electrocatalysts depict excellent performance for both HER and OER, a device for the best performing sample was assembled to determine its overall water splitting performance. The NF || NF electrolyzer achieves the current of 10 mA at 1.665 V, compared to that the STFP01 || STFP01 electrolyzer achieved the same at only 1.638 V as can be seen in Fig. 4-8 (e).

Table 4-3 – Resistances obtained from impedance spectroscopy measurements

SAMPLE ID	**R_S (Ω)**	**R_{CT} (Ω)**	**C_2 (E^{-4} F)**
STF	0.8706	0.3063	3.694
SPTF1	1.293	0.4322	4.899
SPTF2	1.228	0.3657	3.89
STFP1	0.9615	0.05959	6.59
STFP2	0.9276	0.2155	4.222

Table 4-4 - Comparison of recent studies conducted on perovskites as electrochemical catalysts for water splitting

Catalyst	Electrolyte	OER		HER		Reference
		Overpotential (mV)	Taffel slope (mV/dec)	Overpotential (mV)	Taffel slope (mV/dec)	
STF	1M KOH	327.6	112	218.4	77	This work
SPTF1	1M KOH	308.6	112	195.4	158	This work
SPTF2	1M KOH	302.6	104	199.4	136	This work
STFP1	1M KOH	277.6	73	182.4	77	This work
STFP2	1M KOH	285.6	93	198.4	129	This work
$Pr_{0.5}Sr_{0.5}FeO_{3-\delta}$	0.1M KOH	170	-	-	-	[8]
$LaCa_2Fe_3O_8$	1M KOH	36	74	40	143	[9]
Sr_2IrO_4	0.5M H_2SO_4	245	47.4	18.2	30.6	[10]
$La_{0.5}Sr_{0.5}CoO_{3-\delta}/MoSe_2$	0.1M KOH	370	74	200	34	[11]
$(PrBa_{0.5}Sr_{0.5})_{0.95}Co_{1.5}Fe_{0.5}O_{5+\delta}$/3DNG	0.1M KOH	320	74	230	124	[12]
CoP-$PrBa_{0.5}Sr_{0.5}Co_{1.5}Fe_{0.5}O_{5+\delta}$	1M KOH	340	81.5	-	-	[13]

Summary

In this chapter, the results are presented and discussed in detail. The physiochemical properties of the electrocatalysts determined through characterization techniques are first presented. The electrochemical performance of the water-splitting catalysts has also been presented, discussed and compared with recent studies.

References

[1] M. Freeda *et al.*, “Preparation and Characterization of Praseodymium doped Calcium Aluminate nanophosphor ($CaAl_2O_4$:Pr) by sol-gel method.,” 2017, doi: 10.1016/j.matpr.2017.02.130.

[2] J. Al Boukhari *et al.*, “Structural and electrical investigations of pure and rare earth (Er and Pr)-doped NiO nanoparticles,” *Appl. Phys. A Mater. Sci. Process.*, 2020, doi: 10.1007/s00339-019-3247-8.

[3] S. Yurdakal *et al.*, “Chapter 4 - (Photo)catalyst Characterization Techniques: Adsorption Isotherms and BET, SEM, FTIR, UV–Vis, Photoluminescence, and Electrochemical Characterizations,” in *Heterogeneous Photocatalysis - Relationships with Heterogeneous Catalysis and Perspectives*, 1st ed., G. Marcì and L.B.T.-H.P. Palmisano, Eds. Netherlands: Elsevier, 2019, pp. 87–152.

[4] H. Sun *et al.*, “Designing High-Valence Metal Sites for Electrochemical Water Splitting,” *Adv. Funct. Mater.*, vol. 31, no. 16, pp. 1–44, 2021, doi: 10.1002/adfm.202009779.

[5] R. Khan *et al.*, “3D hierarchical heterostructured LSTN@NiMn-layered double hydroxide as a bifunctional water splitting electrocatalyst for hydrogen production,” *Fuel*, 2021, doi: 10.1016/j.fuel.2020.119174.

[6] S. Anantharaj *et al.*, “Amorphous Catalysts and Electrochemical Water Splitting: An Untold Story of Harmony,” *Small*. 2020, doi: 10.1002/smll.201905779.

[7] M. M. Baig *et al.*, “Binder-free heterostructured MWCNTs/Al_2S_3 decorated on NiCo foam as highly reversible cathode material for high-performance supercapacitors,” *Electrochim. Acta*, vol. 340, p. 135955, 2020.

[8] S. Ward *et al.*, “Boosting the oxygen evolution activity in non-stoichiometric praseodymium ferrite-based perovskites by A site substitution for alkaline electrolyser anodes,” *Sustain. Energy Fuels*, 2021, doi: 10.1039/d0se01278e.

[9] S. B. Karki *et al.*, “Bifunctional Water-Splitting Electrocatalysis Achieved by Defect Order in $LaA_2Fe_3O_8$(A = Ca, Sr),” *ACS Appl. Energy Mater.*, 2021, doi: 10.1021/acsaem.1c02028.

[10] L. Zhang *et al.*, “$SrIrO_3$ modified with laminar Sr_2IrO_4 as a robust bifunctional electrocatalyst for overall water splitting in acidic media,” *Chem. Eng. J.*,

2021, doi: 10.1016/j.cej.2021.129604.

[11] X. Wang *et al.*, “High-Performance Platinum-Perovskite Composite Bifunctional Oxygen Electrocatalyst for Rechargeable Zn–Air Battery,” *Adv. Energy Mater.*, 2020, doi: 10.1002/aenm.201903271.

[12] Y. Bu *et al.*, “Synergistic interaction of perovskite oxides and N-doped graphene in versatile electrocatalyst,” *J. Mater. Chem. A,* 2019, doi: 10.1039/c8ta09919g.

[13] Y. Q. Zhang *et al.*, “In situ grown cobalt phosphide (CoP) on perovskite nanofibers as an optimized trifunctional electrocatalyst for Zn-Air batteries and overall water splitting,” *J. Mater. Chem. A,* 2019, doi: 10.1039/c9ta08936e.

Chapter 5: Conclusion and Recommendations

5.1 Conclusions

The following conclusions can be derived from this study:

1. $Sr_2TiFeO_{6-\delta}$ (STF) and Pr-doped STF were synthesized using the Pechini method. Praseodymium was doped at A and B-site of STF to obtain $Sr_{1.9}Pr_{0.1}TiFeO_{6-\delta}$, $Sr_{1.8}Pr_{0.2}TiFeO_{6-\delta}$, $SrTiFe_{0.9}Pr_{0.1}O_{6-\delta}$, and $SrTiFe_{0.8}Pr_{0.2}O_{6-\delta}$.
2. XRD analysis of the samples proved that the samples synthesized all possessed a double perovskite structure. The SEM images of the samples proved that the electrocatalyst had a sponge-like porous structure.
3. In this study, STFP1 stood out amongst all the other samples showcasing the best performance in terms of an OER overpotential of 277.6 mV at 5 mV/s, an HER overpotential of 182.4 mV at 5 mV/s, a charge transfer resistance (R_{CT}) of 0.05959 Ω and a Faradaic capacitance of 6.59 E^{-4}.
4. The overall excellent performance of the samples can be attributed to their double perovskite structures, which demonstrate various benefits when it comes to the formulation of an effective electrocatalyst for water splitting due to its stability in harsh catalytic environments.
5. The sponge-like, porous morphology of the STF structure enhances its ability to facilitate HER and OER by providing a higher surface area for catalytic reactions as proven from the BET analysis.
6. Double perovskite materials may very well be the answer to cost-effective water splitting solutions and should be explored further, especially with stability hand-in-hand with performance.

5.2 Recommendations

It is important that further studies be carried out to further evaluate the performance of double perovskites structures in electrocatalytic water-splitting. Following are some of the recommendations for future studies:

1. Classes of double perovskite other than STF should also be studied. Double perovskites are highly versatile and tunable structures than have proven to be very effective in applications such as solid oxide fuel cells (SOFC) and hydrogen production through methane decomposition.
2. These materials can also be studied for other electrochemical applications apart from water-splitting. Their tunability may aid in applications such as super capacitors and batteries.
3. The effect of varying parameters such as the electrolyte, use of glassy carbon as the electrode and ink preparation techniques could give further insight into the effect these variables have on the performance of this electrocatalyst.

Acknowledgement

All praises and thanks are for Almighty ALLAH, to whom we should bow down, the creator and source of all knowledge and wisdom endowed to mankind, Who guides and helps us in all difficulties and darkness.

I am thankful to my supervisor, Dr. Mustafa Anwar, for the exceptional oversight, inspiration, and advice. I am grateful for his continuous support throughout this journey. I am especially thankful to the principal investigator, Prof. Dr. Zuhair S. Khan, of advanced energy materials lab, Dr. Zuhair S. Khan, along with the lab engineers Mr. Asghar Ali, Mr. Amir Naseem Satti, Mr. Ali Abdullah, and Mr. Qamar-ud-Din for their constant help and assistance throughout the experimentation and research phase.

I am indebted to Prof. Dr. Naseem Iqbal for his support and guidance throughout my research. I would also like to thank Dr. Asif Hussain Khoja for his unparalleled guidance during this period which helped me learn a lot from him.

Thank you

Qassam Sarmad

Appendix A - Publication

Journal of Environmental Chemical Engineering 10 (2022) 107609

Contents lists available at ScienceDirect

Journal of Environmental Chemical Engineering

journal homepage: www.elsevier.com/locate/jece

Praseodymium-doped $Sr_2TiFeO_{6-\delta}$ double perovskite as a bi-functional electrocatalyst for hydrogen production through water splitting

Qassam Sarmad [a], Uneeb Masood Khan [a], Mutawara Mahmood Baig [b], Muhammad Hassan [a], Faaz Ahmed Butt [c], Asif Hussain Khoja [d], Rabia Liaquat [a], Zuhair S. Khan [a], Mustafa Anwar [a,*], Muhammed Ali S.A. [e,*]

[a] Department of Energy Systems Engineering, US-Pakistan Center for Advanced Studies in Energy (USPCAS-E), National University of Sciences and Technology (NUST), H-12, Islamabad 44000, Pakistan
[b] School of Chemical and Materials Engineering (SCME), National University of Sciences and Technology (NUST), H-12, Islamabad 44000, Pakistan
[c] Department of Materials Engineering, NED University of Engineering and Technology, Karachi, Pakistan
[d] Department of Thermal Energy Engineering, US-Pakistan Center for Advanced Studies in Energy (USPCAS-E), National University of Sciences and Technology (NUST), H-12, Islamabad 44000, Pakistan
[e] Fuel Cell Institute, Universiti Kebangsaan Malaysia, UKM, Bangi, 43600, Malaysia

ARTICLE INFO

Editor: Despo Kassinos

Keywords:
Water splitting
Double perovskite
Hydrogen evolution reaction (HER)
Oxygen evolution reaction (OER)
Hydrogen production

ABSTRACT

Water Splitting by electrocatalysis is one method of attaining sustainable production of hydrogen as a clean and promising energy source. Previous studies have shown that perovskite can be effective electrocatalyst for overall water splitting. Herein, double perovskites being highly stable structures have been reported to perform exceptionally in harsh electrochemical environments. The Praseodymium (Pr) doped Strontium Titanium Ferrite (STF) electrocatalyst was tested as an electrocatalyst for water splitting with conductive nickel foam. Pr was doped both on A and B sites of the STF's double perovskite structure, and the $SrTiFe_{0.9}Pr_{0.1}O_{6-\delta}$ (STFP01) showed the best results with an oxygen evolution reaction (OER) overpotential of 277.6 mV @ 5 mV/s and a hydrogen evolution reaction (HER) overpotential of 182.4 mV @ 5 mV/s with low Tafel slopes of 73 mV/dec and 77 mV/dec, respectively. The sponge-like structure of Pr-doped STF exhibits excellent potential to be a viable electrocatalyst while providing a stable structure.

1. Introduction

Fossil fuels are depleting and would not last even for the foreseeable future as the primary energy source in the world. Researchers have long been trying to find alternative fuels, that are sustainable and eco-friendly. Hydrogen leads this race as a potential source of energy that can sustainably cater to the needs of the world. H_2 gas has an extremely high energy density of approximately 142 MJ/kg, and upon combustion, it only produces water as the by-product making it highly clean[1], [2]. Hydrogen is the most abundant element in the known universe; however, it rarely exists on its own as H_2 gas. And hence it must be produced by some other means and stored so that it can be used effectively as and when needed.

Hydrogen or H_2 as fuel can be categorized according to its production method and how clean these methods are. In other words, methods producing the most Carbon can be classified as "grey", methods involving Carbon Capture and Storage (CCS) can be classified as "blue", and methods that emit zero carbon are "green"[3]. This classification helps in identifying the impact H_2 production has on the environment. Traditionally, "grey hydrogen" is produced from techniques such as coal gasification, steam reforming of methane, partial oxidation of methane, and methane decomposition. These techniques are cheaper at this point in time, but they leave a considerable amount of carbon footprint on the environment which defeats the purpose of hydrogen as a clean fuel for the future. "Blue hydrogen", uses the same techniques as "grey hydrogen" but at the same time, it employs carbon capture and storage techniques (CCS). Lastly, "green hydrogen" is the cleanest of the three as it uses techniques that produce H_2 gas purely from water through electrocatalysis, photocatalysis, photoelectrocatalysis, or similar methods that use electricity to split water in H_2 and O_2 gases [4], [5]. "Grey hydrogen" is the most economical right now, however, "blue hydrogen" can pave the way for the future until "green hydrogen"

* Corresponding authors.
E-mail addresses: mustafa@uspcase.nust.edu.pk (M. Anwar), mas@ukm.edu.my (M.A. S.A.).

https://doi.org/10.1016/j.jece.2022.107609
Received 29 December 2021; Received in revised form 12 March 2022; Accepted 21 March 2022
Available online 26 March 2022